Chem Soc Rev

This article was published as part of the

2008 Chemistry at Surfaces issue

Reviewing the latest developments in surface science

All authors contributed to this issue in honour of the 2007 Nobel Prize winner Professor Gerhard Ertl

Please take a look at the issue 10 table of contents to access the other reviews

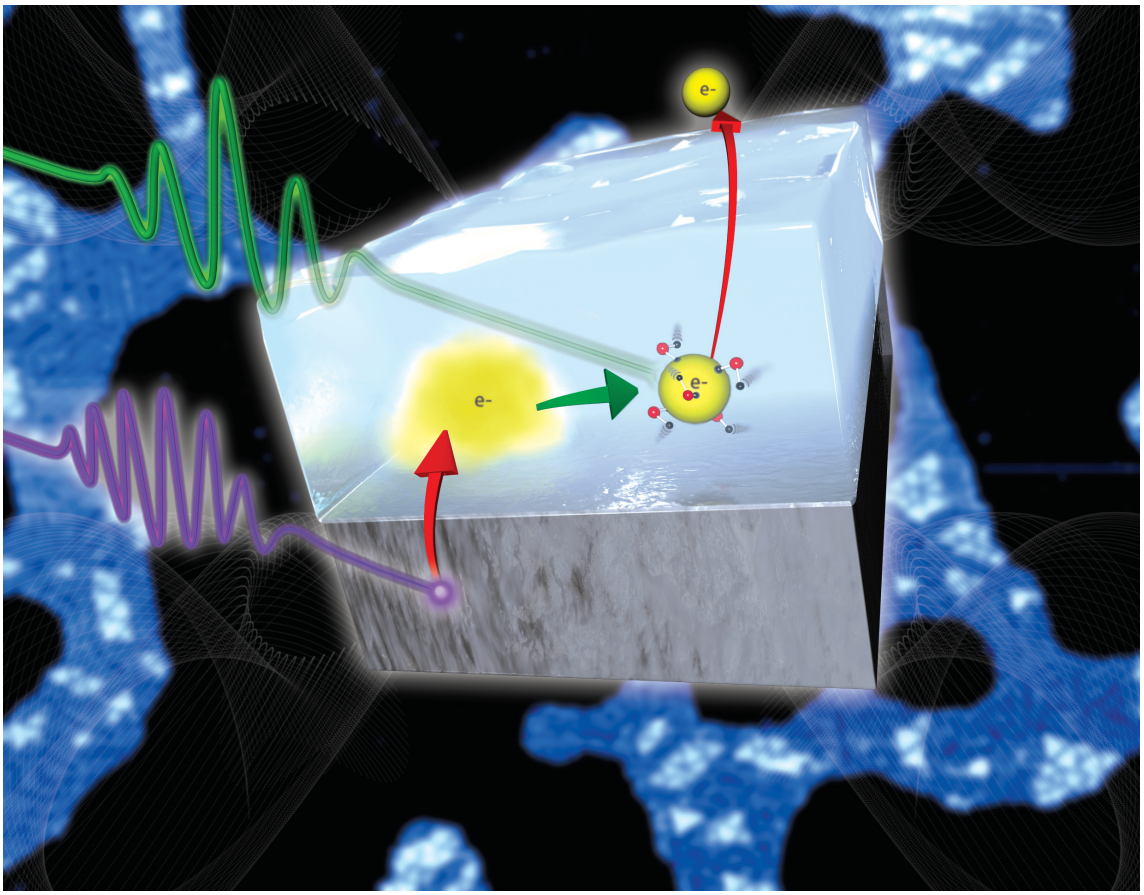

Unraveling molecular transformations on surfaces: a critical comparison of oxidation reactions on coinage metals†

Xiaoying Liu,[a] Robert J. Madix*[b] and Cynthia M. Friend[ab]

Received 1st August 2008
First published as an Advance Article on the web 18th August 2008
DOI: 10.1039/b800309m

The coinage metals, copper, silver, and gold, have unique characteristics for selective oxidation catalysis, particularly for partial oxidation of alcohols and olefins. A basic understanding of surface chemistry at the molecular level can help facilitate the improvement of current catalytic processes and the designing of new catalytic systems. In this *critical review*, the current state of knowledge of these reactions is reviewed. First, both the experimental and theoretical methods necessary for understanding surface reactivity are discussed with a specific set of examples directly related to these reactions. Next the state of understanding of the surface chemistry of the oxidation reactions of alcohols and olefins on these three coinage metals is reviewed and the reaction pathways are compared. Clear relationships between the low pressure surface science studies and more practical catalytic conditions are illustrated. Finally, recent theoretical advances in this area are discussed as well as possible future directions in this field (132 references).

1. Introduction

Metal-catalyzed heterogeneous oxidation has long been of academic and industrial interest. Partial oxidation of alcohols and hydrocarbons, in particular, is of immense importance because it provides large-scale manufacturing of both commodity chemicals and valuable precursors for many specialty processes. For example, transformation of methanol to formaldehyde is achieved by silver catalysts; epoxidation of ethylene with supported silver particles has become a mature industrial process applied world wide.

As economically significant as heterogeneously catalyzed partial oxidation is, this process still faces a number of challenges. A significant problem is improving the selectivity, for instance against the total combustion to CO_2 and H_2O. In the conversion of ethylene to epoxide, for example, the selectivity, though high, is currently limited to approximately 90%,[1] and selectivity increases, even small ones, are of immense value. Another intriguing difficulty is that the rational design of catalytic systems is the exception rather than the rule; to date, progress in heterogeneous catalysis mainly relies on "trial and error" studies. Design requires detailed knowledge of the reaction mechanism and the rate constants for rate-limiting steps in the catalytic processes and further understanding of the reactivity of different catalytic materials.

[a] *Department of Chemistry and Chemical Biology, Harvard University, 12 Oxford Street, Cambridge, MA 02138, USA*
[b] *School of Engineering and Applied Sciences, Harvard University, 29 Oxford Street, Cambridge, MA 02138, USA. E-mail: rmadix@seas.harvard.edu; Fax: 01 617-496-8410; Tel: 01 650-279-6818*

† Part of a thematic issue covering reactions at surfaces in honour of the 2007 Nobel Prize winner Professor Gerhard Ertl.

Robert J. Madix and Gerhard Ertl

Xiaoying Liu received her BS in Chemistry and MS in Inorganic Chemistry from Fudan University, China. She is currently working on her PhD in Physical Chemistry at Harvard University under the supervision of Professor Cynthia M. Friend. Her research interests include mechanistic studies of selective functionalization of olefins and oxidation of alcohols on single-crystal surfaces.

Robert Madix pioneered the use of metallic single crystal as model catalysts for the study of the kinetics and mechanism of partial oxidation reactions. At Stanford University he developed the description of these reactions based on acid–base principles that has broad applicability. For this work he received the Alpha Chi Sigma award of the AIChE and the Adamson Award of the ACS.

Cynthia Friend, Professor of Chemistry and Materials Science at Harvard University, is known for her research on the fundamental study of the chemical and physical properties of surfaces. She recently discovered a rich chemistry of reactions of organic molecules with atomic oxygen adsorbed on model gold catalyst surfaces and the direct aziridination of olefins by adsorbed amide.

Recently, there has been tremendous interest in developing new reaction processes to realize the goal of "green chemistry" that can maximize product yield, reduce energy consumption, and minimize pollution. Heterogeneous catalysis has the potential to play a central role in such processing.

A basic understanding of surface chemistry at the microscopic level includes the identification of reaction intermediates, the determination of the elementary reaction steps, the measurement or calculation of rate constants and reaction energetics for rate-limiting steps, the understanding of surface–adsorbate bonding, and the identification of catalytically active sites. With this understanding, there is hope for directing the reactions through the desirable pathways intelligently, combining experiment and theory.

With the advent of surface-sensitive analytical techniques and the development of methods for determining the identity of rate-limiting active intermediates and the rate constants governing their reactions, there has been substantial development in the molecular-level understanding of the reactions on well-defined surfaces. They provide unambiguous identification of the elementary steps and reaction networks involved in catalytic reactions. The challenge is to elucidate these reaction networks and then to apply this knowledge to the more complex conditions of operation.

2. Methodology

In the past three decades, a parallel development of surface analytical techniques under ultrahigh vacuum and methods for studies of kinetics and mechanism has occurred that allows basic problems of catalytic reactions on surfaces to be addressed. Catalytic reactions are the result of pathways provided by the surface that are energetically inaccessible in the gas phase. Thus, reactions proceed *via* a sequence of elementary steps, often in competition, involving specific, metastable intermediates bound to the surface. Often these intermediates can be isolated and their reactions studied in detail, affording the necessary information to understand complex catalytic cycles. In this section, the chemical methods and a few of the most powerful spectroscopic methods are highlighted, followed by a brief discussion of relevant theoretical methods.

2.1 Experimental techniques

2.1.1 Temperature programmed reaction spectroscopy (TPRS). Temperature programmed reaction spectroscopy is the method used for the elucidation of catalytic cycles on well-defined surfaces. It affords the identification of reaction products and the rate-limiting reactive intermediates leading to their formation, and is the primary tool for the determination of kinetic parameters. In this discussion, we focus on the use of this technique to identify gas phase products, probe reaction intermediates, and determine the rate constants of surface reactions.

Temperature programmed reaction spectroscopy relies on quantitative mass spectrometry. With this method reactants are first dosed onto the surface at a temperature low enough to preclude reaction; the surface is then heated linearly. The products evolving from the surface are detected mass spectrometrically as a function of temperature. Separate reaction channels, having different activation energies are separated on the temperature axis with a resolution of approximately 0.1 kcal mol^{-1}. Generally, this resolution is sufficient to clearly define the reactions involved.

The identification of products proceeds as follows. First, the entire range of possible mass fragments is scanned with low resolution. For this purpose a multiplexed quadrupole mass spectrometer is normally used. Then, having identified the fragments present, the resolution of the mass spectrometer is increased and fewer masses are monitored in subsequent experiments. Often the identity of the reactants suggests the potential products, assisting in identification. A complete initial search is necessary.

In order to further identify the products from a temperature programmed reaction spectrum, their mass spectrometric fragmentation patterns must be known. This pattern can be determined by monitoring all the ions formed when desorbing a multilayer of that species from the surface (having condensed layers of the desired molecule at the appropriately low temperature) or by scanning the fragment distribution while leaking the gas into the vacuum system. In some cases, published tables of fragmentation patterns, such as those from the NIST database,[2] must be judiciously used.

It is most helpful to first identify the parent ion of the product. For most reactions this is straightforward, though in many cases the signal intensity may be low. For a single product isolated by the temperature programmed reaction spectra, once the parent ion is identified, the fragmentation pattern observed for this species at this temperature is compared to the pattern expected from potential products of that total mass, using neat samples of these species for calibration. This process reveals the identity of the product, and excludes other species. In addition, the use of reactants substituted with D, ^{18}O, or ^{13}C helps determine the number of H, O, or C atoms in the product observed and provides a method for tracking the reactivity of particular groups within the molecule. Naturally abundant ^{13}C in the species may also be utilized.

When the product peaks are well separated along the temperature axis, they can be identified one by one as discussed above. But when two or more evolve at the same temperature or overlap in temperature, a more sophisticated analysis is required. In that case, one must solve a set of linear equations for each of the masses (more precisely, mass to charge ratios) observed where the total intensity of each mass is given by the appropriately weighted sum of the contribution of each of the species.[3,4] This is a straightforward procedure if all the products and their corresponding cracking patterns are known. In practice, it is usually possible to identify one of the products based on one unique mass fragment, subtract the contribution of each of its cracking fragments from the other masses observed and proceed to identify all the products. Such a deconvolution may be greatly assisted by identifying one species first by means of isotope labeling. On some occasions, however, one has to solve (usually no more than two) simultaneous equations to separate the contributions of two products at an identical temperature.

A good example of the use of this methodology is the identification of the gas phase products in the reaction of

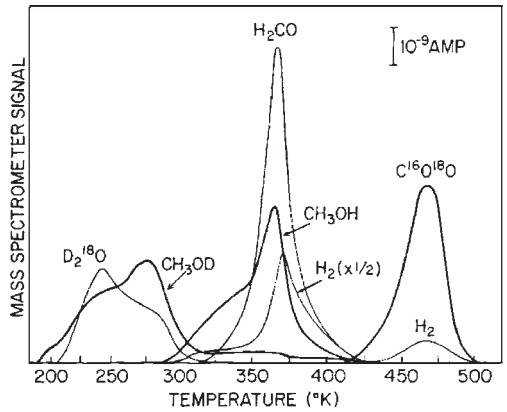

Fig. 1 Temperature programmed reaction spectroscopy of the oxidation of CH_3OD by ^{18}O on a Cu(110) surface.[5]

methanol with atomic oxygen on Cu(110).[5] In order to assist product identification, CH_3OD and ^{18}O were used. As shown in Fig. 1, the two forms of methanol can be distinguished by monitoring m/z 33 for CH_3OD and m/z 31 for CH_3OH, respectively, since in the mass spectrometer CH_3OD gives rise to intense signals at m/z 33 (CH_3OD), 32 (CH_2OD), 29 (CHO), and 15 (CH_3), while for CH_3OH m/z 32, 31, 29, and 15 are expected. H_2CO can be readily identified from the m/z 30 signal because neither species of methanol shows a substantial fragment of m/z 30. $H_2C^{18}O$, though not produced in this reaction, can be distinguished from the fragment of $CH_3OH(D)$ by simultaneously monitoring the magnitude of the m/z 15 fragment. Given the information above, the products in the temperature range of 350–400 K, namely H_2CO, CH_3OH, and H_2 (m/z 2) can be readily distinguished from each other. Other products include $D_2{}^{18}O$ and $C^{16}O^{18}O$. The other two isotopes of water, $HD^{18}O$ and $H_2{}^{18}O$ were excluded since $HD^{18}O$ was not observed (m/z 21), and no residual contribution to the m/z 20 signal was obtained after correcting for the $^{18}OD^+$ contribution from $D_2{}^{18}O$. Distinguishing the isotopes of carbon dioxide is straightforward, as they do not give overlapping fragments; they can be identified by m/z 48 for $C^{18}O^{18}O$, 46 for $C^{16}O^{18}O$, and 44 for $C^{16}O^{16}O$.

Isotope labeling is also invaluable for deducing molecular-level detail related to reaction pathways by analyzing the isotopic distribution of specific mass fragments. Thus, for example, one can distinguish the location of oxygen within a complex molecular product as the result of a catalytic process. In their studies on the oxidative reaction of furan on Ag(110), Crew and Madix employed ^{18}O and furan-d_4 to identify each of the partially oxidized species, namely maleic anhydride, bifuran, and benzene.[6] The isotopic labeling experiments showed that ring-opening of furan must be involved in the formation of maleic anhydride, and accordingly, a reaction pathway that proceeds through the 2-butene-1,4-dial surface intermediate was deduced (Scheme 1).

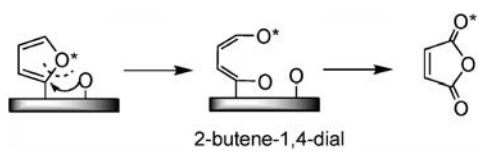

Scheme 1 The ring opening mechanism in the oxidation of furan to form maleic acid (schematic).

Rate-limiting steps can be identified by selective isotope labeling. A corollary of the product identification is the identification of the intermediate from which it derives. Reaction products that evolve at identically the same temperature with the same peak shape (normalized to equal height) must originate from the same reactive intermediate. The reasoning is basic; to exhibit this coincidence they must originate with exactly the same kinetics, hence originate in the same rate-limiting step and have a common precursor. Examples of this are numerous, and some are discussed in following sections, but a simple example is the simultaneous formation of formaldehyde and hydrogen from C–H bond scission in adsorbed methoxy, as illustrated in Fig. 1.

The synthesis of intermediates *via* alternative routes may be also used to establish their participation in a reaction. The strategy is to synthesize an intermediate and then compare their temperature programmed reaction spectra to those observed from different reactants. For example, in the oxidation of methanol on Cu(110), H_2 and CO_2 are observed at the temperature of 470 K.[5] The evolution temperature, activation energy, and pre-exponential factor of CO_2 production, and the ratio of H_2 : CO_2 are identical to those obtained from the decomposition of a formate intermediate, $HCOO_{(a)}$, formed by dissociation of the O–H bond in HCOOH on a clean Cu(110) surface.[7] The ratio of H_2/CO_2 is measured to be $\sim$0.5, providing strong evidence for the formation of a stable surface formate species. This intermediate is also observed as a stable surface species in the oxidation of H_2CO on Cu(110).[8]

Temperature programmed reaction spectroscopy also affords the extraction of the kinetic parameters for the rate-limiting steps measured. The methods employed for kinetic analysis borrow from temperature programmed desorption.[9,10] It is precisely these steps that are most important in estimating the rates of complex catalytic reactions in microkinetic modeling.[11–18] The direct measurement of the reaction rate, the simple experimental setup, and the easy control of the experimental parameters all contribute to the usefulness of this technique. For elementary surface reactions, the kinetic parameters can usually be evaluated employing two strategies based on the Polanyi–Wigner model (eqn (1)): the integral approach and the differential approach.[19] One of the integral procedures defined by Redhead utilizes a solution of eqn (1) for $\theta(T, t)$ using trial parameters of E and v assuming both of them are coverage independent.[9]

$$-\mathrm{d}\theta/\mathrm{d}t = v\theta^n \exp(-E/RT) \quad (1)$$

where, θ is the coverage of the reactant, v the frequency factor, n the reaction order, and E the activation energy.

In another method presented by Chan, Aris, and Weinberg (CAW), E and v can be directly calculated from a single experiment.[20] In contrast to the integral approach where all the calculations are based on one temperature programmed reaction curve, the differential analysis requires a series of experiments in order to construct an Arrhenius plot from which E and v can be readily derived for a given θ.[19] This can be accomplished by varying either the initial reactant

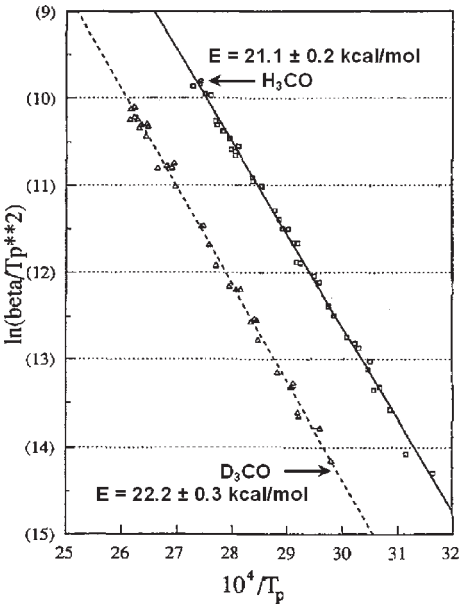

Fig. 2 Heating rate variation plots for the decomposition of isotope-labeled methoxy to formaldehyde. The separation in the lines reflects different symmetry factors in the methyl group and the change in activation energy due to the kinetic isotope effect.[21]

coverage or the heating rate for a constant initial coverage. Leading edge analysis is another differential tactic that is quite useful.[19] Since the coverage change is very small at the leading edge of the evolving curve, the assumption that E and v are coverage-independent holds, thus allowing the direct determination of the kinetic parameters. By analyzing the desorption curves with different initial coverages, the coverage dependency of E and v can be obtained. In the final analysis, the rate parameters must be tested for a range of coverages, so that the integral methods can only be viewed as a starting point.

As an example, heating rate variation was used to determine activation energies and pre-exponential factors and to deduce kinetic isotope effects for the C–H bond scission of methoxy on Cu(110) (eqn (2)).[21]

$$\ln(\beta/T_p^2) = -E/RT_p + \ln(vR/E) \qquad (2)$$

where β is the heating rate (dT/dt), and T_p is the observed peak temperature.

The Arrhenius plots of $\ln(\beta/T_p^2)$ *versus* $1/T_p$ (Fig. 2) were obtained for the production of H_2CO from CH_3O and D_2CO from D_3CO by measuring the peak temperatures as a function of heating rate from 0.06 to 6 K s^{-1}. The rate constants for these two isotopes are $(0.8 \pm 0.3) \times 10^{12}$ exp[(-21.1 ± 0.2) kcal mol^{-1}/RT] s^{-1} and $(0.8 \pm 0.3) \times 10^{12}$ exp[(-22.2 ± 0.3) kcal mol^{-1}/RT] s^{-1}, respectively, consistent with the expected difference in zero point energies and a reactant-like transition state.

Two spectroscopic methods complement temperature programmed reaction spectroscopy particularly well for the determination of reaction mechanism; namely, X-ray photoelectron and vibrational spectroscopies. The useful aspects of these analytical tools are described briefly below, and relevant examples of their use are given in later sections.

2.1.2 X-Ray photoelectron spectroscopy (XPS). Mechanistic analysis by temperature programmed reaction spectroscopy relies on the evolution of products into the gas phase. Techniques which probe the *adsorbed* species significantly expand the scope of our understanding of surface reactions. Coupled with temperature programmed reaction spectroscopy, they provide important supplementary information for the identification of surface intermediates, and (in the case of X-ray photoelectron spectroscopy) a quantitative measure of their surface concentrations. Changes in the binding environment of the atom result in changes in the binding energy of the electrons, so that, in some cases, the evolution of specific surface species can be tracked. For example, the O 1s bonding energy has been widely used to identify oxygen-containing species such as the alkoxy on Cu(110) and to observe its progressive oxidation to formate.[22] Further, in the oxidation of methanol on Cu(110), upon the adsorption of methanol onto the oxygen-covered surface at 140 K, the O 1s peak for preadsorbed oxygen shifts from 530.0 to 531.7 eV, indicating the strong hydrogen bonding between methanol and surface oxygen. When the surface is heated to 270 K to isolate methoxy (as shown by temperature programmed reaction data), a binding energy shift to 530.8 eV is clearly observed. In addition, the ratio of the O 1s peak from the adsorbed methoxy to that of the preadsorbed oxygen is close to the expected value 2 : 1.

2.1.3 Vibrational spectroscopy. The use of vibrational spectroscopies, primarily high-resolution electron energy loss spectroscopy (HREELS) and infrared reflection absorption spectroscopy (IRAS), also aids in the identification of reaction intermediates and allows one to probe their transformation and symmetry on the surface.

High-resolution electron energy loss spectroscopy has been extensively used mainly because of its extremely high sensitivity and broad spectral range. Furthermore, it can be used to circumvent the dipole selection rules that limit the modes observable with infrared spectroscopy. Even at a resolution of only around 40–80 cm^{-1} (as in standard practice) this method enables the identification of specific vibrational modes of adsorbed species, allowing reaction sequences on the surface to be followed. One of the earliest applications of electron energy loss spectroscopy to surface reactions was by Sexton, who showed that when methanol is condensed on the oxygen precovered Cu(100) surface, the vibrational spectrum looks very similar to the infrared spectrum of the gaseous methanol, and when the surface is warmed up to 370 K, intense vibrational bands of C–C and C–O stretching as well as Cu–O stretching and C–H bending are observed (Fig. 3).[23] This spectrum is as expected for methoxy, corroborating earlier temperature programmed reaction studies described above.[5]

Infrared reflection absorption spectroscopy has superior resolution, typically 4 cm^{-1}, and hence allows the vibrational modes to be well resolved. In addition, the dipole selection rule strictly applies, thus the peak intensities can in principle be used to determine molecular orientation and symmetry—important parameters for describing bonding and for comparison to theoretical results. The major disadvantages of this technique are its lower sensitivity and limited spectral range

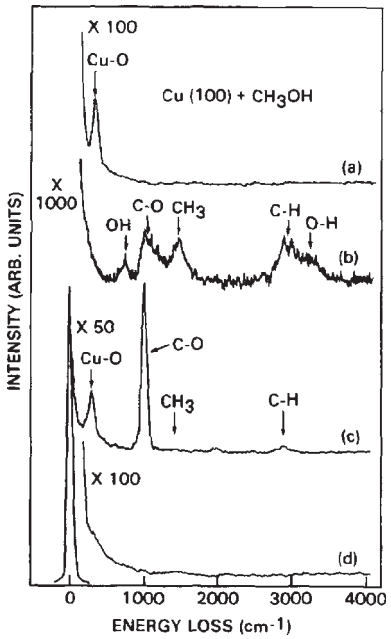

Fig. 3 High-resolution electron energy loss spectroscopy for the reaction of methanol with the oxygen-covered Cu(100) surface. (a) Oxygen-covered Cu(100); (b) multilayer of methanol condensed on the surface (a) at 100 K; (c) warmed up to 370 K; and (d) warmed up to 420 K. All spectra were recorded at 100 K with the beam energy of 5 eV.[23]

($\sim$800–4000 cm^{-1}). Camplin and McCash investigated the geometry of methoxy on a Cu(110) surface using infrared spectroscopy (Fig. 4).[24] The peak at 984 cm^{-1} is assigned as ν_{CO}, the 2810 cm^{-1} band as symmetric methyl stretch ν_{CH}(s), 2883 cm^{-1} as a coupled overtone, and the highest frequency 2920 cm^{-1} as a combination band. The assignment is corroborated by the spectra of the deuterium substituted methoxy, whereas ν_{CO} stays relatively the same, ν_{CD}(s) shifts to 2054 cm^{-1}. A new feature at 1095 cm^{-1}, assigned as δ_{CD}(s) mode, appears due to the close frequency and thus strong coupling with the ν_{CO} mode. Application of the metal surface selection rule to both of the spectra indicates that the C–O bond lies perpendicular to the surface, and the methoxy species adopts an upright configuration on the surface.

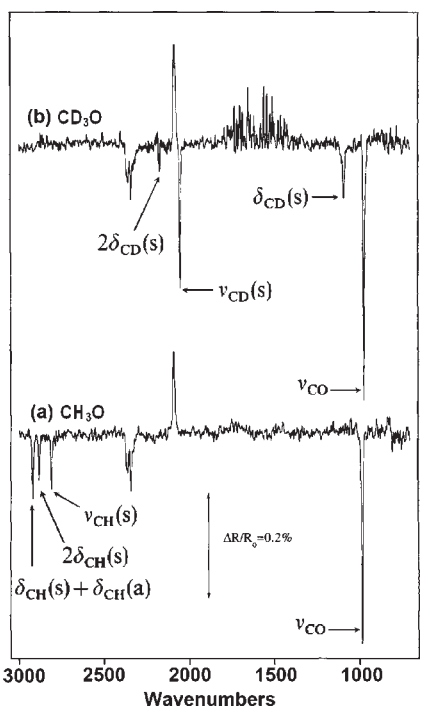

Fig. 4 Infrared spectra of the methoxy species (a) CH_3O and (b) CD_3O on Cu(100) at a surface temperature of approximately 210 K.[24]

2.1.4 Scanning tunneling microscopy (STM). Scanning tunneling microscopy provides atomic information recorded locally on surfaces, in contrast to the statistical behavior over many molecules or atoms obtained from other methods. Owing to its ability to bring the atomic picture to life in surface science studies, STM affords the understanding of local chemical environments during the adsorption and reaction processes that may escape detection by other surface analytical techniques.

As silver, copper and gold surfaces have been shown to reconstruct upon adsorption of atomic oxygen, and since these surfaces are the initial conditions for studies of reactions of alcohol oxidation on the coinage metals, a brief discussion of these structures is warranted.

Adsorbed oxygen on Ag(110) and Cu(110) incorporates metal atoms into its structure, forming rows of –O–Ag–O– or –O–Cu–O– chains running along the [001] direction.[25,26] At saturation coverage they form (2×1) structures (Fig. 5).[27]

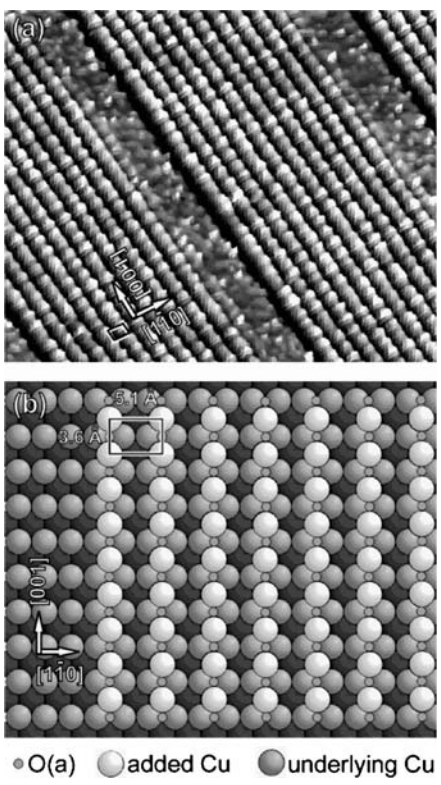

Fig. 5 Scanning tunneling microscopic image (top) of the $p(2\times1)$-O structure on the Cu(110) surface and a ball model (below) showing the added –O–Cu–O– rows.[27]

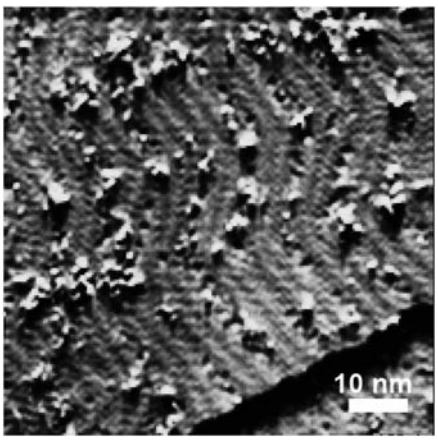

Fig. 6 Scanning tunneling microscopic image of the oxygen-covered Au(111) surface obtained after exposure to ozone at a surface temperature of 200 K, showing the formation of small islands. The oxygen coverage is $\sim$0.2 ML.[28]

Oxygen adsorption on Au(111) causes precipitation of the excess gold at the elbows in the herringbone structure into small clusters, believed to contain adsorbed oxygen, leading to erasure of the herringbone and formation of quasi-ordered 2-D gold oxide phases (Fig. 6).[28] On both silver and gold, heating causes recombinative desorption of dioxygen near 600 K.[29]

STM has been used in studying the structures of more complex systems. For instance, with the composition and structure of the intermediate species identified with other methods such as TPRS, XPS, and HREELS, as discussed above in detail, STM images have been used to investigate the details of chemical reactions on surfaces, such as site specificity and reaction kinetics. It has revealed complex interactions between reactants/reaction intermediates and surface atoms and has shown how surfaces participate in reactions. These applications of STM will continue to grow in importance in the future.

2.2 Theoretical studies

Advances in the theoretical treatment of surface phenomena may allow a more complete and detailed understanding of reactions by providing an independent assessment of the identity of intermediates and transition states for their reactions. With such understanding, microkinetic analysis can predict rates, activation energies, pressure and temperature dependencies, and reaction orders.[11–18] At least at this time, these methods must be considered as complementary to experiments. In the longer term, they may help realize the rational design of heterogeneous catalysts. Advances have been made using density functional theory (DFT) in combination with low pressure mechanistic studies, and specific examples are discussed below which pertain to the understanding of either the kinetics or mechanism of the oxidation reactions on the coinage metals. Most recently, kinetic Monte Carlo (kMC) methods have been developed to model reactive processes on surfaces. These theoretical methods are valuable for understanding bonding and bond activation that are important in catalytic processes and have predictive value when placed in a broad context.

3. Review and comparison of the three metals for oxidation reactions

3.1 Oxidative dehydrogenation of alcohols

The hydroxyl group, OH, is the primary functionality of aliphatic alcohols and shows greater gas phase Brønsted acidity than water. As a result, the reactions of alcohols on oxygen-covered surfaces are initiated by the activation of O–H bonds by adsorbed atomic oxygen to form adsorbed alkoxy and water. Subsequent reaction steps involve C–H bond scission; the differences in the product distributions of different alcohols depend on the structure of the alkyl groups as well as the oxygen coverage.

3.1.1 Oxidation of alcohols on silver. The reactions between alcohols and surface oxygen atoms have been extensively examined on silver single-crystal surfaces. In the oxidation of methanol on Ag(110) studied by Wachs and Madix using temperature programmed reaction spectroscopy, methoxy is readily formed (eqn (3)) upon its adsorption at 180 K as a result of the acid–base reaction between the O–H bond and the surface oxygen atom.[30] It further reacts *via* three pathways: C–H bond scission to form formaldehyde and hydrogen (eqn (5)), recombination with a surface hydrogen atom to form methanol (eqn (6)), and reaction with adsorbed formaldehyde to yield methyl formate and hydrogen *via* the adsorbed H_2COOCH_3 intermediate (eqn (7) and (8)). At low coverages of methoxy, formaldehyde is liberated at 300 K, but due to lateral interactions among adsorbates, at higher coverages formaldehyde is also formed between 200 and 250 K (Fig. 7). The activation energies for the rate-limiting steps can be found in Table 1. Furthermore, the ratio of oxygen atoms to surface methoxy is found to strongly affect the final product

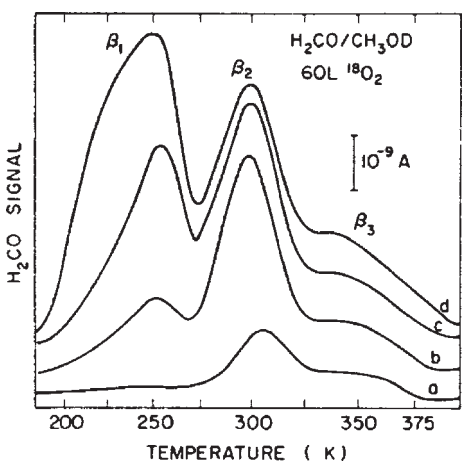

Fig. 7 Temperature programmed reaction spectra for formaldehyde formation obtained following increasing exposure of a Ag(110) surface precovered with ^{18}O to CH_3OD at 180 K to form increasing coverage of adsorbed CH_3O. The CH_3OD exposures were (a) 5 s, (b) 13 s, (c) 25 s, and (d) 75 s. Isotope-labeled oxygen and methanol were used in order to distinguish the origin of oxygen and hydrogen atoms in various products.[30]

Table 1 Activation energies of the evolution of different products in the oxidation of alcohols on silver, copper, and gold surfaces. Their corresponding peak temperatures are given in the parentheses. The peak temperatures and activation energies listed are for the dominant reaction channel for each product at the low coverage of the rate-limiting reactive intermediate. For comparison, the activation energies are calculated from the peak temperature assuming the rate-limiting step is first-order with the pre-exponential factor ν 10^{13} s^{-1}, correcting for differences in the heating rate in different experiments. More precise values of the pre-exponential factors are given in the references

Products on Ag	E/kcal mol^{-1}	Products on Cu	E/kcal mol^{-1}	Products on Au	E/kcal mol^{-1}
Methanol/Ag(110)[30]		**Methanol/Cu(110)**[5]		**Methanol/Au(110)**[60]	
$HCOOCH_3$	16.3 (280)			$HCOOCH_3$	14.7 (250)
H_2CO	17.6 (300)	H_2CO	22.4 (365)		
CO_2	23.8 (402)	CO_2	29.0 (470)	CO_2	20.8 (350)
Methanol/Ag(111)[31]		**Methanol/Cu(111)**[41]			
H_2CO	18.1 (290)	H_2CO	24.1 (382)		
CO_2	22.0 (350)	CO_2	30.1 (474)		
Ethanol/Ag(110)[32]		**Ethanol/Cu(110)**[32]		**Ethanol/Au(111)**[63]	
CH_3CHO	16.0 (273)	CH_3CHO	18.7 (316)		
				$CH_3COOCH_2CH_3$	13.5 (230)
Allyl alcohol/Ag(110)[33]		**Allyl alcohol/Cu(110)**[4]		**Allyl alcohol/Au(111)**[65]	
Acrolein	18.5 (310)	Propanal, acrolein	26.9 (435)	Acrolein	15.1 (255)
***tert*-Butyl alcohol/Ag(110)**[3]		***tert*-Butyl alcohol/Cu(110)**[39]			
Isobutylene oxide, isobutylene	30.8 (510)	Isobutylene	36.7 (600)		
Cyclohexanol/Ag(110)[34]					
Cyclohexanone	18.4 (300)				
Ethylene glycol/Ag(110)[35,36]					
CH_2O	17.9 (300)				
OCHCHO	22.8 (380)				
CO_2	25.0 (415)				

distribution. In the presence of excess oxygen, as shown in Fig. 8, formaldehyde is further oxidized to formate, HCOO, which subsequently yields CO_2 and H_2O with the assistance of surface oxygen (eqn (10), (11), and (12)).

$$2CH_3OH_{(g)} + O_{(a)} \rightarrow 2CH_3O_{(a)} + H_2O_{(a)} \quad (3)$$

$$H_2O_{(a)} \rightarrow H_2O_{(g)} \quad (4)$$

$$CH_3O_{(a)} \rightarrow CH_2O_{(a)} + H_{(a)} \quad (5)$$

$$CH_3O_{(a)} + H_{(a)} \rightarrow CH_3OH_{(g)} \quad (6)$$

$$CH_2O_{(a)} + CH_3O_{(a)} \rightarrow HCOOCH_{3(a)} + H_{(a)} \quad (7)$$

$$HCOOCH_{3(a)} \rightarrow HCOOCH_{3(g)} \quad (8)$$

$$2H_{(a)} \rightarrow H_{2(g)} \quad (9)$$

$$CH_2O_{(a)} + O_{(a)} \rightarrow HCOO_{(a)} + H_{(a)} \quad (10)$$

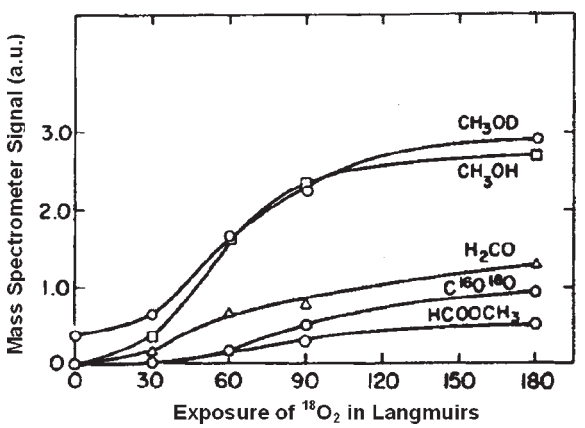

Fig. 8 The evolution of products following saturation doses of CH_3OD onto Ag(110) predosed with varying amounts of $^{18}O_2$. Note that the formation of formaldehyde proceeds the formation of both CO_2 and methyl formate.[30]

$$HCOO_{(a)} \rightarrow CO_{2(g)} + H_{(a)} \quad (11)$$

$$2H_{(a)} + O_{(a)} \rightarrow H_2O_{(g)} \quad (12)$$

Studies of the oxidation of methanol on Ag(111) exhibit many similarities with that on Ag(110) with the exception of the absence of the $HCOOCH_3$ product on Ag(111), as reported by King *et al.*[31] In these experiments, no methyl formate was observed, possibly due to lower surface coverages of methoxy. Two stable reaction intermediates, namely methoxy and formate, were identified using infrared reflection absorption spectroscopy. The reaction of methoxy to formaldehyde also takes place, which desorbs simultaneously with methanol and H_2 at 290 K in a single reaction-limiting step characterized by a first-order activation energy of $\sim$18 kcal mol^{-1} (Table 1).[30] Further oxidation of formaldehyde to formate, which decomposes at 350 K to yield CO_2 and H_2, occurs in the presence of excess surface oxygen. The differences in detail of these two studies may be due to different relative coverages of methanol and oxygen. The multiple peaks for formaldehyde formation on Ag(110) are strongly suggestive of lateral repulsive interactions due to high coverage of the methoxy. Further, since the formation of methyl formate results from reaction of formaldehyde with "excess" alkoxy, it would be favored under high initial coverage of the alkoxy. However, multiple peaks are not observed on Ag(111).[31] The sequential nature of this reaction is illustrated in Fig. 8, which shows that the formation of formaldehyde precedes that of methyl formate. These differences have not been examined further.

Ethanol reacts with adsorbed atomic oxygen in a fashion similar to that of methanol. At low initial oxygen coverages, the adsorbed ethoxy reacts by β-C–H scission in a single rate-limiting step near 275 K (25 K lower than the corresponding reaction of methoxy) to yield acetaldehyde.[32] Some of the hydrogen atoms released recombine to form gaseous H_2, and the rest of them combine with ethoxy to form ethanol. The

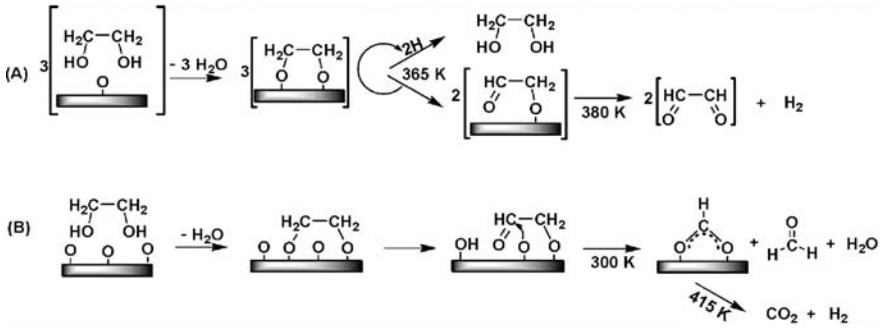

Scheme 2 Reaction scheme for the oxidation of ethylene glycol on Ag(110) (A) under oxygen lean conditions and (B) with excess surface oxygen.[35,36] The curved arrow indicates the surface-mediated transfer of H from one dioxy to another.

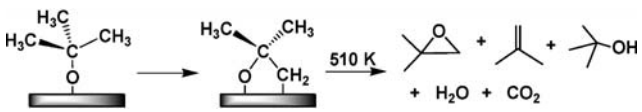

Scheme 3 Reaction of *tert*-butoxy through the oxametallacycle intermediate to form isobutylene oxide, isobutylene, *tert*-butyl alcohol, H_2O, and CO_2 at 510 K.[3]

same reaction pattern also applies to the reaction of other more complicated aliphatic alcohols that possess β-C–H bonds, including primary alcohols such as allyl alcohol,[33] secondary alcohols such as cyclohexanol,[34] and even diols such as ethylene glycol.[35] Aldehyde or ketone is formed as the main partial oxidation product (Table 1) following the activation of the O–H bond. In the case of diols, excess oxygen can react with one of the oxygen-bound carbons, leading to C–C bond activation and the formation of aldehyde and adsorbed carboxylate (Scheme 2).[36,37] Both of these species ultimately lead to CO_2 and H_2O in excess oxygen.

In the case of tertiary alcohols there is no β-H; therefore the alcohols exhibit quite different surface chemistry subsequent to the formation of the alkoxy species due to the initial O–H bond scission by adsorbed oxygen. As shown by Brainard and Madix in the oxidation of *tert*-butyl alcohol on Ag(110), *tert*-butoxy reacts at significantly higher temperatures (510 K) in the absence of coadsorbed oxygen due to the greater difficulty of activation of the methyl C–H bonds (γ-C–H bonds) to yield isobutylene oxide and isobutylene as the major products together with *tert*-butyl alcohol, water, and CO_2.[3,38] The reactions of $(CH_3)_3COH$, $(CH_3)_3COD$, and $(CD_3)_3COH$ show that the production of isobutylene oxide and isobutylene involves the rate-limiting breaking of the C–H/D bond. This observation is a clear indication of the formation of an oxametallacycle intermediate from *tert*-butoxy (Scheme 3) that is also involved in the oxidation of *tert*-butyl alcohol on Cu(110).[39] The higher reaction temperatures are in good accord with the higher bond strength of the γ-C–H bonds as compared to β-C–H bonds. In general, β-C–H bonds are weaker by 4–7 kcal mol^{-1} due to their proximity to oxygen.[3] In the presence of coadsorbed oxygen, the γ-C–H bonds are much less stable, undergoing scission, presumably assisted by oxygen, at 440 K.

3.1.2 Oxidation of alcohols on copper. Oxidation reactions of alcohols have also been well documented on copper surfaces. Alkoxy species are identified as the most abundant surface intermediate, showing a parallel initial activation step to that on silver. In no case does preadsorbed oxygen appear *necessary* to activate the O–H bond, but in the case of methanol it appears necessary to prevent recombination of the methoxy and adsorbed hydrogen, thereby allowing the formation of formaldehyde from C–H bond scission. Preadsorbed oxygen does appear to increase the amount of adsorbed alkoxy formed, however.[22] The surface chemistry of alkoxy exhibits many similar characteristics with that on Ag surfaces; however, slight differences are observed in their relative reaction kinetics, as will be discussed below.

The oxidation of methanol displays a very similar reaction mechanism on Cu(110)[5] as on Ag(110),[30] with essentially the same reaction sequence; however methyl formate is *not* observed (see section 3.1.1). It is believed that the formation of methyl formate is related to the residence time of formaldehyde on the surfaces.[30] Since the Ag(110) surface is more active for the decomposition of the methoxy species, with the activation barrier $\sim$5 kcal mol^{-1} lower than that on Cu(110)[30,5] (Table 1), formaldehyde forms on Ag(110) during temperature programmed reaction at a lower temperature and thereby has a longer surface residence time with which to react with adsorbed methoxy than on Cu(110), resulting in the production of methyl formate. The energetics of the evolution of CO_2 from C–H bond scission in formate also differ: on Cu(110) it forms at 470 K, while on Ag(110) it forms at 402 K, giving a difference of $\sim$5 kcal mol^{-1} in the activation energies, assuming the reaction is first order with a pre-exponential factor of 10^{13} s^{-1} (Table 1).

It is important to note that the reaction scheme is the same on the other two most stable copper facets, Cu(100)[40] and Cu(111),[41] despite their differences in structure. As shown in Table 1, the activation barriers for the evolution of formaldehyde and CO_2 are essentially the same on whichever surface they were measured. This strongly indicates that the oxidation reactivity of alcohols has little dependence upon the surface structure. The same conclusion has also been reached in the oxidation of formic acid *via* formate on copper surfaces.[42,43]

On Cu(110), the reaction of methanol or formic acid to form methoxy or formate, respectively, causes reconstruction of the (2×1)-O structure into a more complex surface reconstruction which may contain added copper atoms interacting with the methoxy or formate intermediate.[44–49] Fig. 9 shows the structure of an oxygen-covered Cu(110) surface after exposure to

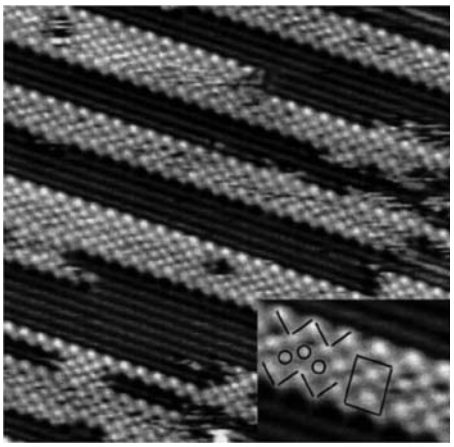

Fig. 9 Scanning tunneling microscopic image (200 Å × 200 Å) of a Cu(110) surface exposed to 1.5 L oxygen followed by a 20 L methanol exposure. This image shows the coexisting methoxy and oxygen structures. Methoxy forms zig-zag chain structures and regions of $c(2\times2)$ periodicities; these two structures can combine to form a (5×2) periodicity.[49]

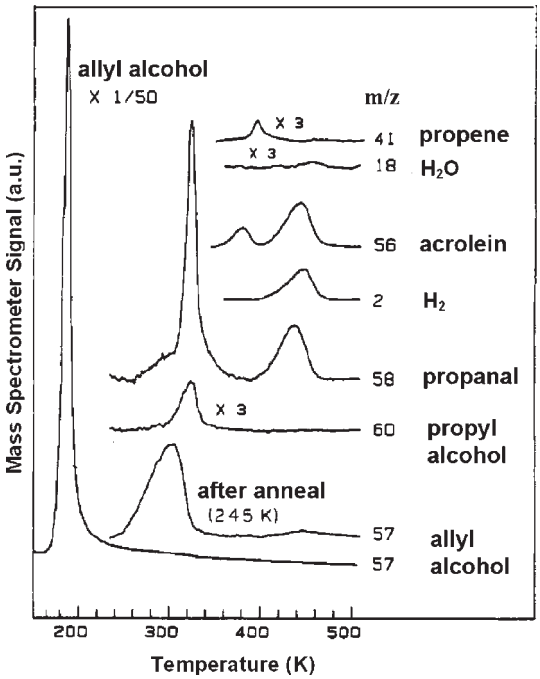

Fig. 10 Temperature programmed reaction spectra for allyl alcohol on a clean Cu(110) surface.[4]

methanol to form methoxy.[49] It is important to realize that these added metal atoms may stabilize these species, influencing the rates of C–H bond scission.

Ethanol oxidation serves as another illustration of the similarities in reaction mechanism and differences in reaction kinetics between Cu(110) and Ag(110).[32] On both surfaces, ethanol is oxidized to surface ethoxy and water upon adsorption at 180 K, and it subsequently decomposes into acetaldehyde and hydrogen. The recombination of surface hydrogen with ethoxy to form ethanol is also observed. Similar to the results in the methanol oxidation, copper is less active than silver for the dehydrogenation of ethoxy to acetaldehyde and hydrogen.[32] For instance, the major acetaldehyde peak occurs at 316 K on copper and 273 K on silver, respectively, corresponding to $\sim$3 kcal mol^{-1} difference in the activation energy for β-C–H bond scission (Table 1).

It is important to point out that due to the strong adsorbate–copper interaction, oxygen-free Cu(110) can activate ethanol, giving rise to the same intermediate species and products as observed on oxygen precovered surface.[32,50] The same pattern of reactivity has been observed for other higher alcohols on clean Cu(110) surfaces, including *n*-propanol, isopropanol, and ethylene glycol.[50] The activation of O–H bonds by adsorbed atomic oxygen leads to the formation of

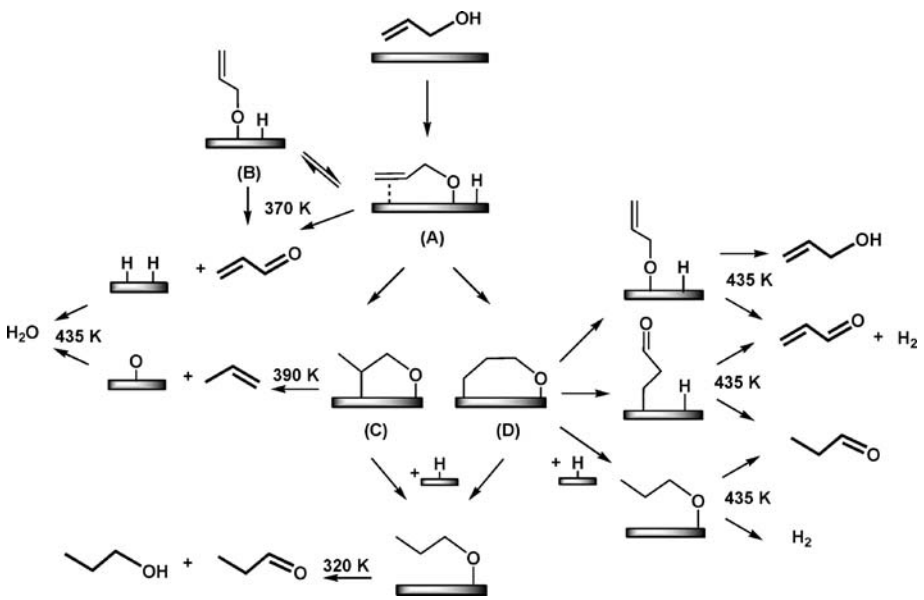

Scheme 4 Reaction pathways of allyl alcohol on the clean Cu(110) surface. The formation of two oxametallacycle intermediates (C and D) is a result of hydrogenation of the double bond by the hydrogen released from initial O–H bond scission. Note that both reaction pathways at 320 and 435 K can yield propanal.[4]

surface alkoxy species that react further with the surface and dehydrogenate to yield the corresponding aldehyde or ketone in the gas phase. On the other hand, adsorbed oxygen increases the yield of aldehyde.

Allyl alcohol, on the other hand, which represents a family of bifunctional alcohols, having both a C=C double bond and the acidic O–H group, reacts quite differently on copper than on silver. On clean Cu(110) surfaces, as noted above, the O–H bond is activated to form adsorbed allyloxy and adsorbed hydrogen atoms. Additionally, the π-bond in the adsorbed allyloxy forms a weak donor bond with the surface, and it is readily hydrogenated by the adsorbed hydrogen released in the activation of the O–H bond. Thus, the allyl alcohol reacts on copper through a variety of pathways that involve the activation of both of its two functionalities, hydroxyl and olefin.[4] As shown in Fig. 10, the allyloxy (A and B in Scheme 4) undergoes β-H elimination to liberate acrolein at 370 K, as with silver. In addition, propanal and propanol are formed from oxametallacycle intermediates (C and D in Scheme 4) resulting from hydrogenation of the double bond *near room temperature* by the hydrogen released from initial O–H bond scission. As can be seen from Scheme 4, both acyclic (low temperature route, 320 K) and cyclic (high temperature route, 435 K) intermediates appear to be involved in propanal formation. This reactivity of copper thus contrasts sharply to the selective oxidation of allyl alcohol to acrolein on oxygen-predosed Ag(110).[33] However, as expected, preadsorbed atomic oxygen on Cu(110) facilitates direct transfer of the hydroxyl hydrogen in the alcohol to the adsorbed oxygen, thereby eliminating O–H bond scission as a source of adsorbed hydrogen and suppressing the low temperature hydrogenation to propanal and propanol. In this case propanal is formed *via* hydrogen released to the surface upon acrolein formation from allyloxy at a higher temperature. The activation energy for β-H elimination from the allyloxy is also substantially higher on Cu(110) (435 K) than Ag(110) (310 K), partly due to the stronger stabilizing interaction of the π-bond in the allyloxy intermediate with the copper surface, though in both cases such bonding is observed.[29,33,51]

3.1.3 Oxidation of alcohols on gold. Alcohol oxidation on gold has not been studied as extensively as for silver and copper, since it was widely accepted that gold would have low reactivity. In the recent years, however, the unique reactivity and selectivity of gold catalysts have attracted the attention of many researchers.[52–54] There has been tremendous interest in the selective oxidation of alcohols—both in the gas and solution phase—due to the wide applications of their derivative carbonyl compounds in chemical industry.[55–59] The oxidation of alcohols on gold surfaces shares some common features with that on silver and copper, but significant differences are observed. The similarity lies in that their surface chemistry also appears to follow a two step process involving the initial low-temperature activation of the acidic O–H bonds followed by the cleavage of the C–H bonds. However, the adsorbed alkoxy species exhibits quite different reactivity.

The oxidation of methanol on Au(110) proceeds *via* the activation of the O–H bond by adsorbed oxygen to form methoxy at 200 K, but only methanol, methyl formate, and water are produced at 250 K, and CO_2 desorbs at 350 K.[60] It is very unusual that gaseous formaldehyde is *not* observed, in sharp contrast with its dominance on Ag(110)[30] and Cu(110)[5,61] surfaces. Rather, the preferred pathway is to the ester, methyl formate (Table 1). This difference may originate from a fundamental difference in the bonding of methoxy to the gold surfaces, rendering it more susceptible to attack by the aldehyde.[60] On gold, methoxy apparently decomposes to adsorbed formaldehyde at 250 K, a temperature lower than that on silver, so that its reaction with adsorbed methoxy to form methyl formate is even more probable due to its longer surface lifetime during heating. On silver or copper, formaldehyde desorbs much faster at the relatively higher decomposition temperatures of methoxy (Table 1), although some methyl formate is observed on Ag(110) at sufficiently high coverages of methoxy.[30] In addition, analogous to the behavior of silver and copper surfaces,[5,30] formate also exists as a stable intermediate on gold through secondary oxidation of formaldehyde. The decomposition temperature of the formate on Au(110) is 350 K, the temperature being lower than that observed on Ag(110) (400 K) and Cu(110) (475 K).[62] The higher decomposition temperatures may be, to some extent, attributed to the surface reconstruction.[45,46,48]

One can see from the proposed mechanism that the decomposition temperature of alkoxy *via* β-H elimination should be lower than the desorption temperature of the aldehyde formed in order for esterification to occur. Indeed, the generality of this mechanism (reaction (13)) has been confirmed by Liu and Friend in their recent investigations on the oxidation of ethanol on the Au(111) surface.[63] When the Au(111) surface is precovered with 0.4 ML atomic oxygen the reaction of ethanol yields ethyl acetate at 230 K and acetic acid at 450 and 545 K (Fig. 11). Molecular acetaldehyde desorbs from the clean gold surface at a slightly higher temperature. In addition, ketene and CO_2 are formed from adsorbed acetate. At oxygen coverages below 0.1 ML, ethyl acetate is the sole product. In

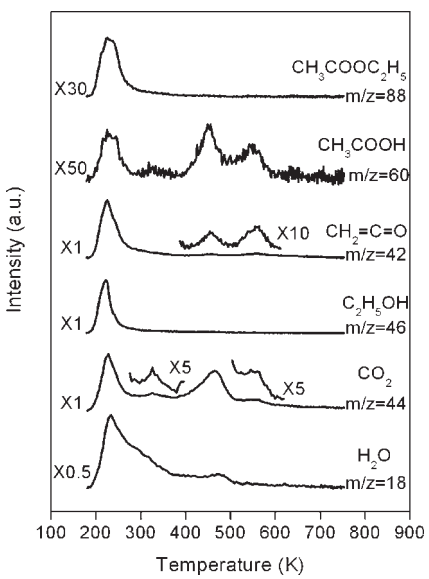

Fig. 11 Temperature programmed reaction spectra for the oxidation of ethanol on Au(111). The surface is precovered with atomic oxygen with the coverage 0.4 ML.[63]

no case is gaseous acetaldehyde formed from these reactions. Moreover, it is found that the yield of ethyl acetate greatly increases when acetaldehyde is co-dosed with ethanol onto the oxygen-covered gold surface, providing direct evidence that its formation is accounted for by reaction (13).

$$RCHO_{(a)} + RO_{(a)} \rightarrow RCOOR + H_{(a)} \qquad (13)$$

It is noteworthy that the above results from ultrahigh vacuum studies on single-crystal gold surfaces are in good agreement with those of ethanol oxidation in aqueous solution at 3.5 MPa pressure over supported gold catalysts.[64] The mechanistic origin of the formation of ethyl acetate and acetic acid under these high pressure, industrial conditions can be well explained by the reaction pathways obtained on single-crystal surfaces, providing an illustration of the link between ultrahigh vacuum studies and heterogeneous catalysis.

Reactions of other alcohols that have been investigated on preoxygenated gold surfaces include allyl alcohol,[65] cyclohexanol,[66] and 2-cyclohexen-1-ol.[67] In these cases only aldehyde or ketone is produced; no ester is formed. Acrolein is formed at 255 K, cyclohexanone at 265 K, and 2-cyclohexen-1-one at 270 K. The two allylic alcohols exhibit more complicated reaction patterns. As exemplified by allyl alcohol, in addition to acrolein, at least two other partial oxidation products are observed, acrylic acid and carbon suboxide. Both of them are considered to be the result of secondary oxidation of the intermediate species acrolein. Dehydrogenation to form carbon suboxide could be facilitated by the planar π system in acrolein that brings all the hydrogen atoms close to the surface and makes them subject to attack by excess surface oxygen.

It is important to add that CO_2 can also react with adsorbed oxygen on silver to form adsorbed carbonate, which is stable to nearly 500 K, at which temperature it decomposes to adsorbed oxygen and gaseous CO_2. Carbonate has not been observed to form on the clean surfaces of either copper or gold.[68] Thus, in any steady state application of silver for selective partial oxidation, temperatures must be sufficiently high to prevent accumulation of carbonate.

In summary, on all of the three group IB coinage metals, adsorbed atomic oxygen reacts with alcohols as a strong Brønsted base; it reacts with the acidic O–H bonds below 200 K leading to the formation of stable adsorbed alkoxy. The subsequent decomposition of the primary and secondary alkoxy usually occurs *via* β-H elimination in the temperature range of 220–400 K to form acetaldehyde or ketone and hydrogen simultaneously. Whether the aldehyde evolves into the gas phase depends on (1) the decomposition temperature of alkoxy, (2) its stability on the metal surfaces, (3) its reactivity with other surface species such as alkoxy or oxygen, and (4) the presence of other functionalities such as the C=C double bond in the alkyl group. As a result of these factors, esters, olefins, and other products can also be formed depending on the specific alcohol. In the oxidation of tertiary alcohols, γ-H activation is enabled, which occurs above 400 K. Furthermore, the product distribution and the reaction selectivity can be controlled, to a certain extent, by varying the initial alcohol : oxygen ratio. In oxygen-lean environments, partial oxidation to the aldehyde or ketone is favored.

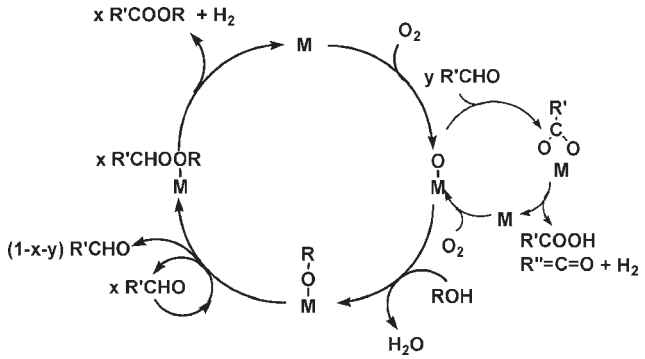

Scheme 5 Catalytic cycle depicting the oxidation of alcohols on copper, silver, and gold surfaces (represented by M). *x* represents the portion of aldehyde that participates in the subsequent esterification reaction. *y* represents the portion of aldehyde that makes the acid. On copper, esterification is not observed, therefore $x = 0$. Combustion cycles are not shown (see text).

Scheme 5 summarizes all the pathways that occur in the oxidation of alcohols on silver, copper, and gold surfaces regardless of the crystallographic facets on which the reaction takes place. The rich chemistry underlying the alcohol oxidation processes allows for the rational synthesis of a large number of derivative compounds. The wealth of mechanistic information that is established can serve as a valuable guide in the design of heterogeneously catalyzed processes.

3.2 Oxidation of olefins

Single-crystal studies of the oxidation reactions of olefins have been greatly motivated by the importance of metal-catalyzed heterogeneous epoxidation processes in the chemical industry. The reactivity of non-allylic olefins *vs.* allylic olefins, especially ethylene *vs.* propene, is a topic of great interest for both fundamental research and applied technologies. Due to the fact that the activation energy for ethylene desorption is lower than that for epoxidation,[69] ethylene epoxide is not formed on coinage metals under ultrahigh vacuum conditions using standard temperature programmed reaction methods following the coadsorption of ethylene with preadsorbed atomic oxygen. However, higher molecular-weight olefins that bind sufficiently strongly with the surface have been studied as model non-allylic olefins; these include norbornene,[69] styrene,[70–75] 3,3-dimethyl-1-butene,[76] and 1,3-butadiene.[77,78] In the same way, allylic olefins including cyclohexene[67,79,80] and phenyl-substituted propene isomers[81–83] have been used to examine the effect of the allylic hydrogens on the selectivity toward epoxidation.

3.2.1 Oxidation of non-allylic olefins. The epoxidation of norbornene was successfully demonstrated under ultrahigh vacuum conditions on the Ag(110) surface by Roberts and Madix in 1988, providing the first direct evidence that atomic oxygen is responsible for the epoxidation reaction of olefins.[69] In the temperature programmed reaction spectra, norbornene oxide is the only partial oxidation product observed together with the formation of H_2O and CO_2. It evolves at a higher temperature (310 K) than its characteristic desorption temperature from either clean or oxygen-covered Ag(110) surfaces, clearly indicating that the rate-limiting step involves a

Table 2 Activation energies for the formation of dominant partial oxidation products in the oxidation of olefins on silver, copper, and gold surfaces. See the caption of Table 1 for details

Products on Ag	E/kcal mol^{-1}	Products on Cu	E/kcal mol^{-1}	Products on Au	E/kcal mol^{-1}
Norbornene/Ag(110)[69]				**Norbornene/Au(111)**[85]	
Norbornene oxide	18.3 (310)			Norbornene oxide	17.5 (295)
Styrene/Ag(100)[90]					
Styrene oxide	27.7 (450)				
Styrene/Ag(110)		**Styrene/Cu(110)**[73]			
Styrene oxide[91]	16.8 (275)	Styrene oxide	23.6 (385)		
Phenylacetaldehyde[70]	34.3 (545)				
Phenylketene[70]	34.6 (550)				
Styrene/Ag(111)[72]		**Styrene/Cu(111)**[74]		**Styrene/Au(111)**[75]	
Styrene oxide	19.9 (330)	Styrene oxide[a]	17.0 (280)	Styrene oxide	20.9 (350)
			24.5 (400)		
Butadiene/Ag(110)[77]		**Butadiene/Cu(111)**[78]			
		Epoxybutene	15.1 (250)		
2,5-Dihydrofuran, furan	26.3 (465)				

[a] Two desorption states with comparable intensity are observed.

rearrangement of an intermediate in which norbornene and oxygen are combined. Similar results with styrene[73] and 3, 3-dimethyl-1-butene[76] soon followed. Subsequent studies in 1990 using a silver powder catalyst and a temporal analysis of products (TAP) reactor confirmed that adsorbed atomic oxygen readily epoxidizes ethylene as well.[84] The generality of this reaction was thus firmly established long ago.

The reaction of norbornene with atomic oxygen on Au(111) surface shows the same reaction products, norbornene oxide, H_2O, and CO_2.[85] The evolution of the epoxide shows a similar activation barrier as that on Ag(110), as shown in Table 2. These results demonstrate that oxygen adatoms show the property of cycloaddition to C═C double bonds on gold, as well as on silver surfaces.

Experimental studies continue to contribute support for the formation of the surface oxametallacycle and its subsequent competing reactions in determining the reaction selectivity of olefins on coinage metal surfaces, as originally proposed by Brainard and Madix.[38,70,71,75,86–88] Linic and Barteau have demonstrated that exposure of the Ag(111) crystal to ethylene oxide at carefully chosen surface temperatures produces a stable surface intermediate *via* ring opening that ring closes at 300 K to reform ethylene oxide and a few other minor products, including ethylene, water, and ethanol.[89] The high-resolution electron energy loss spectra are in good agreement with theoretical calculations based on a surface oxametallacycle. Moreover, the similarity in the activation energies required to form ethylene oxide from this oxametallacycle and in the catalytic epoxidation of ethylene further suggests that the oxametallacycle is actively involved in ethylene epoxidation.

Currently the oxametallacycle intermediate has been widely adopted by researchers to successfully explain the product distribution in the oxidation of olefins. In the partial oxidation of styrene, for example, it has been found that its reactions exhibit strong structure sensitivity on silver single-crystals.[70] On Ag(111)[71,72] and Ag(100)[90] styrene oxide is the partial oxidation product, whereas on Ag(110) phenylacetaldehyde and phenylketene dominate.[70] Furthermore, branching reactions of the oxametallacycle determine the selectivity of

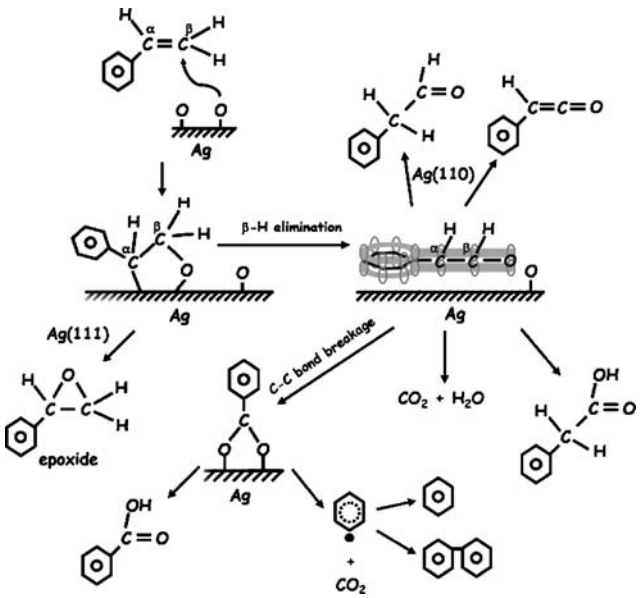

Scheme 6 Reaction scheme of styrene oxidation on silver single crystals.

epoxidation on both Ag(110) and Ag(111). Using X-ray photoelectron spectroscopy, Zhou and Madix have identified the oxametallacycle, a combustion intermediate, and benzoate as intermediates in the oxidation of styrene on both Ag(110) and Ag(111).[91] As shown in Scheme 6, while the oxametallacycle leads to the formation of epoxide, reactions of the combustion intermediate, derived from the oxametallacycle *via* β-H elimination, lead to phenylacetaldehyde, phenylketene, and phenylacetic acid as well as adsorbed benzoate and products derived therefrom. Quantitative analysis of the C 1s and O 1s photoelectron spectra for the reaction on Ag(111) (Fig. 12) and Ag(110) (not shown) clearly shows that the conversion of oxametallacycle to the combustion intermediate is easier on Ag(110) than on Ag(111), leading to the pronounced structure sensitivity for styrene oxide production, which is favored on Ag(111) and short-circuited on Ag(110).

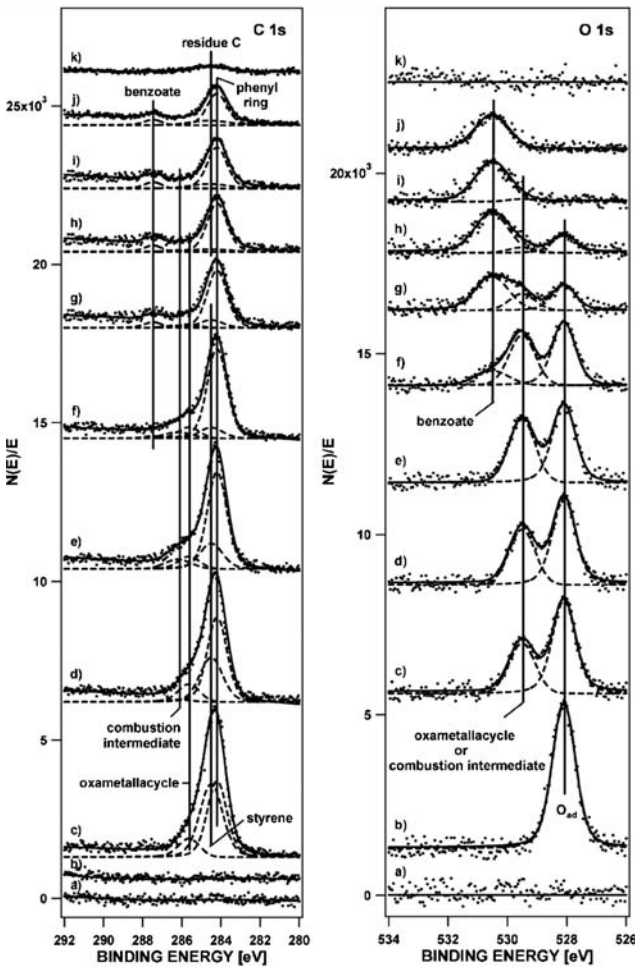

Fig. 12 X-Ray photoelectron spectra (C 1s and O 1s) of a styrene multilayer reacting with a $p(4\times4)$-O covered Ag(111) surface by dosing NO_2 at 470 K; all spectra were taken at 170 K. (a) Clean surface; (b) $p(4\times4)$-O covered surface; (c) after dosing styrene on the oxygen-covered Ag(111) surface at 170 K; and then annealing the surface to (d) 210 K; (e) 230, (f) 250, (g) 280; (h) 320, (i) 350, (j) 450 K, and (k) 650 K. Dots: original data; curve: fitted curve; dashed curve: component peak.[72]

The oxidation of styrene has also been studied on copper and gold. On both Cu(110)[73] and Cu(111),[74] it has been reported that epoxide is observed as the only product, showing no structural sensitivity. It is not evident from these papers if they searched for higher molecular-weight products. On Au(111)[75] the reactivity pattern is similar to that on Ag(111).[71,72] The activation energies for epoxidation on these surfaces are compared in Table 2. Since no investigation has been conducted on other gold surfaces, no conclusions regarding the structure sensitivity can be made.

The selective epoxidation of butadiene is also of considerable importance. 1,3-Butadiene reacts on Cu(111) to form exclusively 3,4-epoxybut-1-ene, its yield being highest at an oxygen coverage of 0.04 ML.[78] The reactivity decreases above this coverage, and is eventually quenched at 0.5 ML where a disordered Cu_2O-like phase is formed on the surface.[92] The inhibition is ascribed to the poor electrophilicity of oxygen as a result of the increase in its charge density upon the formation of metal oxide, though a simpler site-blocking argument is also plausible. It is interesting that the reaction of 1,3-butadiene with atomic oxygen on the Ag(110) surface shows no evidence for epoxide formation; 2,5-dihydrofuran and furan are formed *via* 1,4-cycloaddition.[77] Their evolution commencing at 465 K shows the same kinetics, and is proposed to undergo a disproportionation pathway that involves an allyl intermediate. In addition, small quantities of 2(5*H*)-furanone, maleic anhydride, 4-vinylcyclohexene, and styrene are observed together with combustion products of H_2O and CO_2. 2(5*H*)-Furanone results from further oxidation of 2,5-dihydrofuran.[93] Epoxidation is possible under industrial conditions with *promoted* silver catalysts, however.[94–96]

One can see from the above discussion that the reaction of non-allylic olefins with atomic oxygen on coinage metal surfaces is governed by the cycloaddition character of oxygen, leading to the formation of epoxide or other cyclic adducts that incorporate oxygen atoms in the ring. In the secondary oxidation of surface intermediate species to form acid or anhydride, oxygen also acts as a nucleophile that attacks the electron-deficient carbon atoms.

3.2.2 Oxidation of allylic olefins. Due to the presence of the acidic allylic C–H bonds, the reaction of allylic olefins on coinage metal surfaces is largely dictated by the Brønsted acid–base reaction between allylic hydrogen and surface oxygen. For instance, propene reacts with oxygen on Ag(110) to form H_2O and CO_2 *via* an unstable allyl species that is formed through allylic hydrogen abstraction;[97,98] 2-methylpropene reacts to form a surface trimethylenemethane intermediate which is further oxidized into H_2O and CO_2.[99] Therefore, in the oxidation of propene on silver total combustion is strongly favored.[100] The absence of any epoxide in these cases is attributed to the predominance of the allylic hydrogen activation *via* the acid–base mechanism that in principle competes with oxygen addition to the C=C double bond.

The oxidation of propene shows additional and remarkably different reactions on gold surfaces. Deng *et al*. have observed the partial oxidation products, acrolein, acrylic acid, and carbon suboxide from Au(111), produced in competition with combustion at an initial oxygen coverage of 0.3 ML.[65] Acrolein is the primary partial oxidation product, and is derived through β-H elimination of the allyloxy intermediate that is formed *via* insertion of oxygen into the allylic C–H bond (Scheme 7). This unique intermediate, not observed on silver surfaces, is to be distinguished from the allyl species that leads to total combustion. The oxygen insertion pathway is associated with the presence of distinct oxygen bonding to the surface that appears to have a lower Brønsted basicity than a more ordered phase of oxygen that has reactivity similar to O adsorbed on silver. This oxygen is only present under conditions favoring a disordered, metastable phase of oxygen on

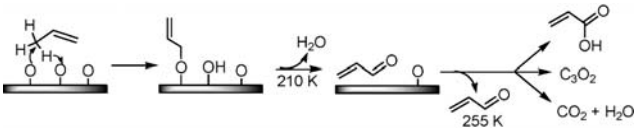

Scheme 7 Selective oxygen insertion in the reaction of propene with atomic oxygen on Au(111).[65]

Au(111), not for an ordered, 2-D surface "oxide".[101] Subsequent nucleophilic attack of excess surface oxygen on acrolein yields the other two products. While no epoxide is formed in the oxidation of C_3H_6, a small amount *is* observed in the reaction of its deuterated counterparts, C_3D_6 and $CD_3CH{=}CH_2$, due to the suppressed reactivity of the allylic C–D bond as a consequence of the kinetic isotope effect. These results strongly indicate the subtle competition of the three reactions: combustion *via* the allyl intermediate, partial oxidation *via* the allyloxy intermediate, and epoxidation *via* the oxametallacycle. This further illustrates the importance of allylic C–H bond activation in determining the product distribution, which is in line with the conclusion drawn from the studies on silver surfaces.[97–99] Davis and Goodman have reported the oxidation of propene with 0.4 ML of atomic oxygen on Au(100) which yields primarily combustion products and a small amount of an unidentified partial oxidation product with molecular weight 56.[102] This product evolves below room temperature and very probably is acrolein, by analogy with Au(111).[65] It should be pointed out that it is possible that all of the partially oxidized species discussed above can further react with excess oxygen to form CO_2 and H_2O, affording additional combustion pathways.

Cyclohexene provides another interesting example of partial oxidation, with important differences on silver and gold surfaces. On both Ag(110)[79] and Ag(111),[80] benzene is the principle partial oxidation product. Roberts and Madix demonstrated that it is formed *via* the sequential abstraction of four hydrogen atoms around the ring, the first allylic C–H bond activation to yield cyclohexallyl apparently being rate-limiting on Ag(110).[79] This sequential process is facile by virtue of π resonance stabilization. However, the reactivity of cyclohexene on Au(111) is distinct from silver, in that, in addition to benzene, 2-cyclohexen-1-one, 2-cyclohexene-1, 4-dione, and phenol are observed.[67] The conversion of cyclohexene to the three oxygenates all require both the activation of allylic hydrogens and the grafting of oxygen atoms to the ring. Liu, Friend and co-workers have shown they are formed *via* 2-cyclohexen-1-oxy, which results from oxygen insertion into the allylic C–H bond of cyclohexene. The formation of this surface species follows a pathway analogous to the formation of allyloxy from propene (Scheme 7),[65] strongly suggesting the generality of this pathway for allylic olefins on Au(111).

More complex higher allylic olefins have also been investigated. Lambert and colleagues have studied the reactivity of the three phenylpropene isomers (their structures shown in Fig. 13), *trans*-β-methylstyrene, α-methylstyrene, and allylbenzene, on Cu(111)[82,83] and Au(111).[103,104] On Cu(111), epoxidation is observed in competition with olefin decomposition to form surface carbonaceous species.[16] Combustion is not a prevalent channel—CO_2 is formed only in the case of α-methylstyrene, probably due to the extremely low oxygen coverage used in all experiments (0.07 ML). Therefore, it can be anticipated that the residual carbonaceous deposit is a result of allylic C–H activation under oxygen lean conditions, and that there is insufficient oxygen to remove the carbonaceous deposit as combustion products. Different patterns of reactivity are observed for these three molecules. *trans*-β-Methylstyrene undergoes extensive epoxidation, accompanied by relatively little decomposition; α-methylstyrene shows some epoxide formation and extensive decomposition; and allylbenzene is almost inert with respect to both reaction channels.

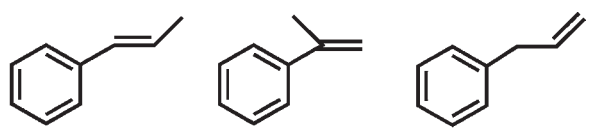

Fig. 13 Structures of the three phenylpropene isomers.

Liu and Friend recently examined the reactivity of the three molecules on oxygen precovered Au(111).[103,104] On Au(111), the oxidation chemistry of these allylic olefins is governed by the same three pathways that are important in propene oxidation: (1) oxygen insertion into allylic C–H bonds, (2) Brønsted acid–base reactions between adsorbed oxygen and allylic protons, and (3) oxygen addition to the C=C bonds to form epoxide, providing direct evidence that both allylic hydrogen activation and epoxidation are competing *partial* oxidation pathways. In addition, nucleophilic attack at the electron-deficient carbon in the asymmetric C=C bonds is observed, giving rise to benzoic acid. It appears that the selectivity for the three isomers toward epoxidation is different, and the pattern parallels that associated with the intrinsic gas phase acidity of these molecules, as determined by density functional theory calculations.[104] Specifically, *trans*-β-methylstyrene and α-methylstyrene show very similar gas phase acidities, and both produce epoxide. However, allylbenzene, being the most acidic among the three, with its ΔG_{acid} value $\sim$50 kcal mol^{-1} lower than the other two, shows no epoxidation.

The pattern for epoxidation of these three phenylpropene isomers is similar on oxidized Cu(111) and Au(111). Specifically, epoxidation of *trans*-β-methylstyrene and α-methylstyrene is induced, whereas no epoxide is detected from the oxidation of allylbenzene. Furthermore, it is clear that the phenyl ring in these molecules has a strong influence on the kinetics for epoxidation *vs*. activation of the allylic C–H bonds since propene epoxidation is not induced by oxygen on either Cu or Au in significant quantities. As in the case of propene, oxygen insertion to form the allyloxy intermediate also occurs for these phenylpropene isomers on Au(111) and is related to a specific form of oxygen on the surface. This pathway was not considered on Cu(111), so it is not possible to determine if this insertion pathway is unique to Au.

Previous studies of *trans*-β-methylstyrene on Ag(100) have shown that only CO_2 and H_2O are produced; no partial oxidation occurs.[81] It is not clear whether this dramatic difference is due to an intrinsic difference in the reactivity between silver, copper, and gold, or because of the difference in the structure of the (100) surface of silver. Nevertheless, epoxide is formed on both Cu(111) and Au(111) surfaces despite the presence of allylic hydrogens. It is noticeable that two different interpretations have been proposed to account for the different reactions of the three isomers, adsorption geometry and gas phase acidity for reactions taking place on

Cu(111)[16] and Au(111),[38] respectively. It seems likely that the reactivity patterns must include effects of the relative gas phase acidities of the three different molecules. While the initial adsorption geometries apparently lead to different proximities of the C=C bond of the three isomers on Cu(111), it is important to recognize that substantial rearrangement is likely to occur upon heating as reaction occurs, making it highly likely that the gas phase acidity plays an important role in determining the barrier height. Further studies are required in order to determine if these two factors work together to control the reactivity of allylic olefins on coinage metal surfaces.

To summarize, atomic oxygen adsorbed on the group IB metals acts as a cycloaddition agent when reacting with C=C bonds and a Brønsted base when abstracting allylic hydrogens, and can insert into C–H bonds to form either adsorbed alkoxy and their analogues or further oxidation products, such as acids. It is interesting to note that the selective oxygen-insertion pathway is reported only on gold, probably indicating its distinct intrinsic reactivity.

3.3 Theory and application of ultrahigh vacuum surface studies to higher pressures and temperatures

A basic understanding of surface chemistry associated with coinage metal-catalyzed heterogeneous oxidation processes and heterogeneous catalysis overall is being established by surface science studies under ultrahigh vacuum conditions. The detailed mechanistic information can serve as a valuable guide for predicting reactivity and selectivity for a variety of reaction processes under vastly different conditions, provided theory can link these disparate conditions. The coinage metals are particularly suitable for connecting fundamental studies and catalysis under operating conditions because of the relatively low steady-state concentration of intermediates present on the surface even under higher pressure conditions. This section is written from the point of view of the experimentalist with the purpose of using theoretical results in combination with idealized experiments for kinetic modeling in practical systems.

Several new approaches are emerging for rational catalyst developments that combine the mechanistic analysis from surface science and various theoretical approaches. Theoretical approaches have successfully been used to model catalytic processes, specifically, microkinetic modeling based on mechanisms and kinetic parameters derived from surface chemistry[17,105,106] and kinetic Monte Carlo (kMC) simulations that use binding energies and barrier heights calculated using density functional theory (DFT).[107–110] *Ab initio* molecular dynamics (MD) simulations of surface reactions would also be an effective tool for studying catalytic processes; however, they have only been applied to the study of Si surface chemistry,[111,112] not to systems of catalytic interest. More commonly, DFT has been used to calculate the binding energies of intermediates to the surface and the barriers for reactive processes in order to draw inferences about reaction selectivity without specifically simulating kinetics.[88,113]

Theoretical studies have the potential to reveal the nature of bonding that gives rise to specific types of bond activation, to probe the nature of the transition state for key reactions, and ultimately to provide quantitative kinetic models for catalytic processes. Development of kinetic models is the ultimate goal of this approach since catalysis is kinetic in nature. While there have already been many advances in this area, there is still a need to advance computational accuracy and speed to fully exploit these emerging methods. To date, there are no reports of kMC or MD simulations of the oxidation reactions on coinage metals that is the topic of this review, most likely due to the relative complexity of these systems. On the other hand, the construction of microkinetic models and the study of key reaction intermediates using DFT have already advanced our understanding of alcohol and olefin oxidation on coinage metals. These theoretical methods have also clearly established that surface chemistry studies at low pressure provide mechanistic information useful for predicting reaction rates at higher pressure.

The starting point for describing catalytic processes is the determination of a detailed reaction mechanism. Surface chemistry studies at low pressure form the foundation for both the microkinetic and kMC approaches because they establish the elementary steps and the nature of surface intermediates present on the surface. Furthermore, the intermediates identified using surface science studies also guide DFT calculations related to catalytic phenomena.

Microkinetic models provide estimates of surface coverages, reaction orders, and activation energies under practical reaction conditions at high pressure and high temperature, hence serving to bridge the so-called "gaps" between surface science and heterogeneous catalysis. Therefore, the close combination of surface science studies and microkinetic modeling appears very promising in the future design and development of catalytic systems.

An important example of this method is the study of methanol oxidation over silver catalysts by Andreasen *et al.*[17] Their model is solely based on the Langmuir–Hinshelwood mechanism with all the elementary steps extracted from the work described above (the Wachs and Madix mechanism) on silver single-crystal surfaces under ultrahigh vacuum conditions. The simulations over a wide range of catalytic reaction conditions reveal no significant deviations when compared to actual data. Hence, such a microkinetic model explains a broad range of reaction parameters including reaction orders, selectivity, and apparent activation energies for realistic conditions.[114] One important result of this simulation is that the coverages of the reaction intermediates in this process are quite low under steady-state reaction conditions. This fact points clearly to the need for the determination of rate constants, such as the pre-exponential factor and activation energy for C–H bond cleavage in methoxy at very low surface coverages. Little information of this kind exists in the literature, but it is readily obtained either from temperature programmed reaction studies or modulated molecular beam methods.[115,116] The parameters necessary to compute equilibrium constants and partition functions, for example, adsorption energies and vibrational frequencies in the case of methanol oxidation over Ag, are derived from experimental data.[17] A similar methodology has also been successfully employed to study and predict the rates of methanol synthesis catalyzed by Cu.[105,106]

Microkinetic models can also be constructed by using energies and reaction pathways derived from DFT calculations. One study of this nature is the investigation of ethylene epoxidation by silver.[117,118] The use of DFT provides parameters necessary for computing the rates of reaction when key parameters are not experimentally available; however, the rates computed are dependent on the accuracy of the bond strengths and vibrational frequencies and, of course, the accuracy of the structures assumed for the reactive intermediates including the configurations of surface metal atoms.

In order to use DFT to formulate kinetic models—whether they be microkinetic kMC, or MD simulations—the energetics of bonding of key intermediates to the surface and of bond breaking and making within intermediates must be determined. The nudged elastic band (NEB) method has been widely used to estimate activation energies for specific reactive processes on the surface.[119] In addition, the nature of bonding of intermediates to the surface can be analyzed—analogous to a frontier orbital analysis for molecular chemistry—in order to develop predictive frameworks.[120–122] Overall, theoretical investigation of the bonding of key surface intermediates, in particular using DFT, is potentially valuable for predicting factors that will change reactions rates and selectivities.

DFT studies of olefin oxidation on the coinage metals provides a good example of how theory can complement experiment in developing models for catalytic systems, but also illustrates some of the potential problems with relying solely on electronic structure calculations. Using DFT, Barteau *et al.* calculated the structure and vibrational frequencies for a two-carbon oxametallacycle bound to a Ag_2 cluster, which compared favorably to measured frequencies for the metallacycle synthesized from iodoethanol.[123] The same intermediate was subsequently formed from ring opening of ethylene oxide on Ag(111).[124] Later, DFT was also applied to the branching reactions of the oxametallacycle intermediate during the oxidation of ethylene, and the epoxidation selectivities were predicted reasonably well.[113,117,125–127] Energetically feasible transition states for the competing reactions assumed to lead to ethylene oxide, respectively, ring closure and a hydrogen shift to form acetaldehyde, which is believed to be responsible for combustion products, were calculated on an Ag_{15} cluster. An activation energy difference of 0.3 kcal mol^{-1} was obtained in favor of the formation of acetaldehyde.[113,117] This difference yields an estimate of the maximum selectivity of 41–43% to ethylene oxide on unpromoted Ag at 400–500 K, in reasonable agreement with typical selectivities reported ranging broadly from 25 to 50%. In contrast, the calculation by Bocquet, Loffreda *et al.* on a $p(4\times4)$ surface oxide adlayer on Ag(111), favored acetaldehyde by almost 2 kcal mol^{-1} in the activation barrier, yielding a selectivity of only 4% to ethylene oxide at 600 K and a partial pressure of 1 atm for both ethylene and oxygen.[125] According to their calculation, a staggered conformation of the oxametallacycle is formed on this surface that actually facilitates hydrogen migration and thus favors the formation of acetaldehyde when subsurface oxygen is present. Subsurface oxygen was also found to be important for ethylene oxidation on Ag(100).[128] In other work, Mavrikakis and Greeley suggested that an ethylene dioxy species plays a role in ethylene oxidation on Ag(111) at high oxygen coverages or when there is subsurface oxygen.[129]

In general kinetic models of this type, regardless of the computation methods used, currently have limitations which must be recognized. For example, the selectivities calculated for ethylene epoxidation on Ag and later on Au[126] and Cu[130] all *assume* that combustion solely occurs *via* acetaldehyde—the "minimum" network proposed by Barteau *et al.*[123] While it is certainly reasonable that combustion will occur through this pathway, it is not necessarily the sole route to combustion, as noted in the work of Mavrikakis, who proposes direct attack of the oxametallacycle by oxygen to form ethylene dioxy, which is known to combust, as described above in section 3.1.1.[35] One of the challenges in using theoretical calculations to understand catalytic processes is to include *all* relevant pathways. In order to accurately describe catalytic processes with any of the possible theoretical methods, all important processes must be evaluated either using theory (DFT) or experiment. Furthermore, such DFT studies would ideally include a frontier orbital analysis of the bonding of these intermediates in order to provide a general understanding of the relationship between bonding and reactivity—especially, the factors that control reaction selectivity.

The large differences resulting from the calculations related to ethylene epoxidation on Ag highlight several important challenges for experiment and theory: (1) to determine reliable estimates of the coverages of the reaction intermediates and oxygen, so as to provide the framework for the rate calculations from DFT; (2) to provide a method to search for global minima over a wider range of configurations of both ground states and transition states. There is a critical need for uniformity in the choice of cluster *vs.* slab calculations and use of an appropriate number of layers in the slabs. For greater accuracy for the microkinetic models, slabs should be adopted. There has been considerable variability in the calculations performed to date for ethylene epoxidation on Ag: the surface was modeled with clusters and with periodic slabs (with different numbers of layers), the oxygen coverage and the amount of subsurface oxygen were also different, and the specific codes and functionals used in the calculations were also often different and not compared directly. Oxygen-assisted processes, important at high oxygen coverages, may be critical or irrelevant, depending on process conditions. Ideally more powerful theoretical approaches that enable construction of a general free energy landscape, rather than the local minima now obtained from the restricted initial conditions imposed, can be developed. Perhaps one of the most important limitations of all DFT calculations to date concerned with olefin oxidation is that they do not include migratory metal atoms that are known from experiment to stabilize reaction intermediates.[131] A first step in this direction was the inclusion of changes in the number of active sites for methanol synthesis over Cu in microkinetic modeling.[106] Migratory metal atoms will very likely play a major role in determining the kinetics and selectivity for many surface reactions, but especially those on coinage metals. Currently, notwithstanding the potential difficulty, it is important to investigate models that include all pathways suggested by experiment and the role of migratory metals atoms if useful connections between theory and practice are to be fully realized.

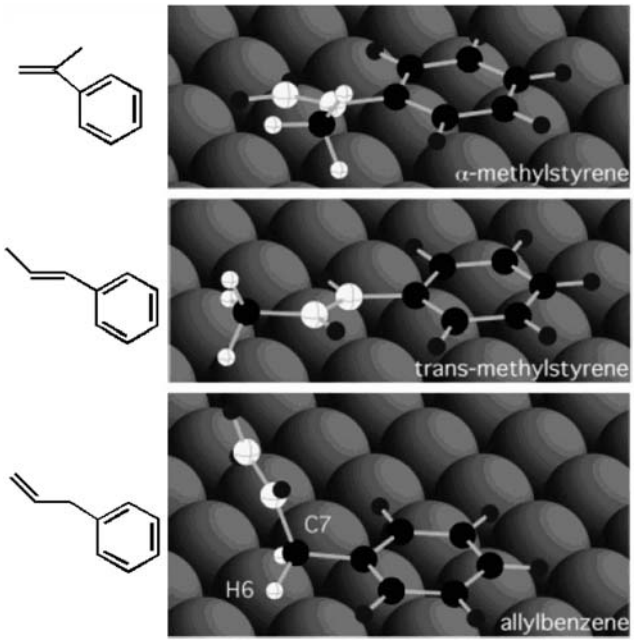

Fig. 14 Adsorption geometry of the three phenylpropene isomers, *trans*-β-methylstyrene, α-methylstyrene, and allylbenzene on the Cu(111) surface as determined by density functional theory calculations.[83]

DFT has also been used to investigate the factors that limit selectivity for epoxidation of olefins with allylic C–H bonds—propene and the various isomers of phenylpropene. DFT calculations were used to investigate the differences in the energetics for propene oxidation on Ag(111) *vs*. Cu(111).[88] A model was constructed in which formation of the oxametallacycle by reaction of propene with adsorbed oxygen competes with allylic C–H bond activation to form allyl, presumed to lead to combustion. As in the case of ethylene, though, only two competing pathways—ring closure to the epoxide and 1, 2-hydrogen shift to form the aldehyde—were considered for reaction of the oxametallacycle. As noted in section 3.2.2 for Au(111), oxygen insertion pathways are possible, and attack of the oxametallacycle by oxygen could also lead to combustion. The barriers for oxygen assisted activation of the allylic C–H bond are different for Cu and Ag. A difference in Lewis basicity of oxygen on these two surfaces is ascribed to the higher selectivity for epoxidation on Cu. Interestingly, there is an energetic preference for addition of oxygen to the terminal olefinic carbon (carbon-1) on both surfaces and the barriers for formation of the oxametallacycle is similar as well, $\sim$0.6 eV. The energetics for the subsequent reactions—ring closure to propene oxide and rearrangement to propanal—have different absolute and relative energies on the two surfaces. The absolute energy barriers for both of these processes are higher on Cu than Ag; however, the ring closure to propene oxide has a somewhat lower barrier than propanal formation on Cu, while the opposite is true for Ag(111).

In another study of the relationship of reactivity to molecular structure, Lambert *et al*. studied phenylpropene isomers on Cu(111) using a cluster model of the surface and DFT.[132] The authors combined DFT calculations and experimental angle-resolved near edge X-ray absorption fine structure (NEXAFS) spectra to demonstrate that the three phenylpropene isomers show different adsorption geometries on the clean Cu(111) surface.[83,132] Specifically, in their lowest energy state both α-methylstyrene and *trans*-β-methylstyrene adopt an essentially planar geometry close to the surface, the vinyl group of α-methylstyrene being closer to the surface, whereas allylbenzene lies with the phenyl group parallel to the surface and the vinyl group directed away (Fig. 14). The proximity of the C=C bonds to the surface is taken to portend a propensity for epoxidation in the order, α-methylstyrene > *trans*-β-methylstyrene > allylbenzene. The other functionality, allylic hydrogen, is also susceptible to attack by surface oxygen, leading to decomposition. Its proximity with respect to the surface is used to explain the relative abundance of the decomposition of *trans*-β-methylstyrene and the relatively inert behavior of allylbenzene. In this case, the barriers for the different processes—oxametallacycle formation *vs*. allylic C–H stripping—were not calculated, and therefore differences in reactivity were inferred from initial state (reactant) binding configurations. In the case of propene on Cu(111) and Ag(111), there was a low barrier for transfer of hydrogen to oxygen for a specific geometric configuration in which the allylic protons interacted with oxygen on the surface.[88] It is probable that similar factors will play a role for the phenylpropene isomers. A more dynamic approach to these problems is needed that accounts for thermal motion in the adsorbed state and differences in the transition state energies of homologous reactants.

In summary, there have been major advances in theoretical methods applied to surface chemistry and catalysis over the past decade. These advances have provided a framework for understanding and improving catalytic processes on the coinage metals, *e.g*. alcohol and olefin oxidation. At the same time, further developments in methodology to accompany anticipated increases in computation speed are needed in order to develop accurate, complete, and dynamic models of catalytic reactions.

Acknowledgements

We gratefully acknowledge the support of this work by the US Department of Energy, Basic Energy Sciences, under Grant No. FG02-84-ER13289, and the National Science Foundation, under Grant CHE 9820703.

References

1 P. I. Chipman, A. M. Madgavkar and G. B. Shipp, *US Pat*., 7 235 677, 2007.
2 S. E. Stein, in *"Mass Spectra" in NIST Chemistry WebBook*, ed. P. J. Linstrom and W. G. Mallard, National Institute of Standards and Technology, Gaithersburg MD, 20899 (http://webbook.nist.gov), June, 2005.
3 R. L. Brainard and R. J. Madix, *J. Am. Chem. Soc*., 1989, **111**, 3826–3835.
4 R. L. Brainard, C. G. Peterson and R. J. Madix, *J. Am. Chem. Soc*., 1989, **111**, 4553–4561.
5 I. E. Wachs and R. J. Madix, *J. Catal*., 1978, **53**, 208–227.
6 W. W. Crew and R. J. Madix, *J. Am. Chem. Soc*., 1993, **115**, 729–736.
7 D. H. S. Ying and R. J. Madix, *J. Catal*., 1980, **61**, 48–56.

8 I. E. Wachs and R. J. Madix, *Surf. Sci.*, 1979, **84**, 375–386.
9 P. A. Redhead, *Vacuum*, 1962, **12**, 203–211.
10 D. A. King, *Surf. Sci.*, 1975, **47**, 384–402.
11 N. Waletzko and L. D. Schmidt, *AIChE J.*, 1988, **34**, 1146–1156.
12 J. E. Rekoske, R. D. Cortright, S. A. Goddard, S. B. Sharma and J. A. Dumesic, *J. Phys. Chem.*, 1992, **96**, 1880–1888.
13 D. A. Hickman and L. D. Schmidt, *AIChE J.*, 1993, **39**, 1164–1177.
14 C. V. Ovesen, B. S. Clausen, B. S. Hammershoi, G. Steffensen, T. Askgaard, I. Chorkendorff, J. K. Norskov, P. B. Rasmussen, P. Stoltze and P. Taylor, *J. Catal.*, 1996, **158**, 170–180.
15 P. Stoltze, *Prog. Surf. Sci.*, 2000, **65**, 65–150.
16 R. D. Cortright and J. A. Dumesic, *Adv. Catal.*, 2001, **46**, 161–264.
17 A. Andreasen, H. Lynggaard, C. Stegelmann and P. Stoltze, *Surf. Sci.*, 2003, **544**, 5–23.
18 C. Stegelmann, N. C. Schiodt, C. T. Campbell and P. Stoltze, *J. Catal.*, 2004, **221**, 630–649.
19 J. B. Miller, H. R. Siddiqui, S. M. Gates, J. N. Russell, J. T. Yates, J. C. Tully and M. J. Cardillo, *J. Chem. Phys.*, 1987, **87**, 6725–6732.
20 C. M. Chan, R. Aris and W. H. Weinberg, *Appl. Surf. Sci.*, 1978, **1**, 360–376.
21 R. J. Madix and S. G. Telford, *Surf. Sci.*, 1995, **328**, L576–L581.
22 M. Bowker and R. J. Madix, *Surf. Sci.*, 1980, **95**, 190–206.
23 B. A. Sexton, *Surf. Sci.*, 1979, **88**, 299–318.
24 J. P. Camplin and E. M. McCash, *Surf. Sci.*, 1996, **360**, 229–241.
25 F. Jensen, F. Besenbacher, E. Laesgaard and I. Stensgaard, *Phys. Rev. B: Condens. Matter Mater. Phys.*, 1990, **41**, 10233–10236.
26 F. Besenbacher and J. K. Norskov, *Prog. Surf. Sci.*, 1993, **44**, 5–66.
27 X. C. Guo and R. J. Madix, *Acc. Chem. Res.*, 2003, **36**, 471–480.
28 B. K. Min, A. R. Alemozafar, D. Pinnaduwage, X. Deng and C. M. Friend, *J. Phys. Chem. B*, 2006, **110**, 19833–19838.
29 R. J. Madix and J. T. Roberts, in *Surface Reactions*, ed. R. J. Madix, Springer-Verlag, Berlin, Heidelberg, 1st edn, 1994, vol. 34, pp. 5–53.
30 I. E. Wachs and R. J. Madix, *Surf. Sci.*, 1978, **76**, 531–558.
31 W. S. Sim, P. Gardner and D. A. King, *J. Phys. Chem.*, 1995, **99**, 16002–16010.
32 I. E. Wachs and R. J. Madix, *Appl. Surf. Sci.*, 1978, **1**, 303–328.
33 J. L. Solomon and R. J. Madix, *J. Phys. Chem.*, 1987, **91**, 6241–6244.
34 P. B. Merrill and R. J. Madix, *Langmuir*, 1991, **7**, 3034–3040.
35 A. J. Capote and R. J. Madix, *J. Am. Chem. Soc.*, 1989, **111**, 3570–3577.
36 A. J. Capote and R. J. Madix, *Surf. Sci.*, 1989, **214**, 276–288.
37 C. R. Ayre and R. J. Madix, *Surf. Sci.*, 1994, **303**, 297–311.
38 R. L. Brainard and R. J. Madix, *J. Am. Chem. Soc.*, 1987, **109**, 8082–8083.
39 R. L. Brainard and R. J. Madix, *Surf. Sci.*, 1989, **214**, 396–406.
40 R. Ryberg, *J. Chem. Phys.*, 1985, **82**, 567–573.
41 J. N. Russell, S. M. Gates and J. T. Yates, *Surf. Sci.*, 1985, **163**, 516–540.
42 M. Bowker and R. J. Madix, *Surf. Sci.*, 1981, **102**, 542–565.
43 B. A. Sexton, *Surf. Sci.*, 1979, **88**, 319–330.
44 S. Poulston, A. H. Jones, R. A. Bennett and M. Bowker, *J. Phys.: Condens. Matter*, 1996, **8**, L765–L771.
45 A. H. Jones, S. Poulston, R. A. Bennett and M. Bowker, *Surf. Sci.*, 1997, **380**, 31–44.
46 S. Poulston, A. Jones, R. A. Bennett and M. Bowker, *Surf. Sci.*, 1997, **377**, 66–70.
47 R. A. Bennett, S. Poulston and M. Bowker, *J. Chem. Phys.*, 1998, **108**, 6916–6922.
48 S. L. Silva, R. M. Lemor and F. M. Leibsle, *Surf. Sci.*, 1999, **421**, 146–156.
49 S. L. Silva, A. A. Patel, T. M. Pham and F. M. Leibsle, *Surf. Sci.*, 1999, **441**, 351–365.
50 M. Bowker and R. J. Madix, *Surf. Sci.*, 1982, **116**, 549–572.
51 J. L. Solomon, R. J. Madix and J. Stohr, *J. Chem. Phys.*, 1988, **89**, 5316–5322.
52 M. Haruta, N. Yamada, T. Kobayashi and S. Iijima, *J. Catal.*, 1989, **115**, 301–309.
53 T. Hayashi, K. Tanaka and M. Haruta, *J. Catal.*, 1998, **178**, 566–575.
54 G. C. Bond and D. T. Thompson, *Catal. Rev. Sci. Eng.*, 1999, **41**, 319–388.
55 L. Prati and M. Rossi, *J. Catal.*, 1998, **176**, 552–560.
56 A. Abad, P. Concepcion, A. Corma and H. Garcia, *Angew. Chem., Int. Ed.*, 2005, **44**, 4066–4069.
57 S. Biella and M. Rossi, *Chem. Commun.*, 2003, 378–379.
58 C. Bianchi, F. Porta, L. Prati and M. Rossi, *Top. Catal.*, 2000, **13**, 231–236.
59 D. I. Enache, D. W. Knight and G. J. Hutchings, *Catal. Lett.*, 2005, **103**, 43–52.
60 D. A. Outka and R. J. Madix, *J. Am. Chem. Soc.*, 1987, **109**, 1708–1714.
61 S. M. Francis, F. M. Leibsle, S. Haq, N. Xiang and M. Bowker, *Surf. Sci.*, 1994, **315**, 284–292.
62 D. A. Outka and R. J. Madix, *Surf. Sci.*, 1987, **179**, 361–376.
63 X. Y. Liu and C. M. Friend, unpublished work.
64 B. Jorgensen, S. E. Christiansen, M. L. D. Thomsen and C. H. Christensen, *J. Catal.*, 2007, **251**, 332–337.
65 X. Y. Deng, B. K. Min, X. Y. Liu and C. M. Friend, *J. Phys. Chem. B*, 2006, **110**, 15982–15987.
66 X. Y. Liu and C. M. Friend, unpublished work.
67 X. Y. Liu and C. M. Friend, unpublished work.
68 F. Solymosi, *J. Mol. Catal.*, 1991, **65**, 337–358.
69 J. T. Roberts and R. J. Madix, *J. Am. Chem. Soc.*, 1988, **110**, 8540–8541.
70 X. Y. Liu, A. Klust, R. J. Madix and C. M. Friend, *J. Phys. Chem. C*, 2007, **111**, 3675–3679.
71 A. Klust and R. J. Madix, *J. Am. Chem. Soc.*, 2006, **128**, 1034–1035.
72 L. Zhou and R. J. Madix, *J. Phys. Chem. C*, 2008, **112**, 4725–4734.
73 J. J. Cowell, A. K. Santra, R. Lindsay, R. M. Lambert, A. Baraldi and A. Goldoni, *Surf. Sci.*, 1999, **437**, 1–8.
74 A. K. Santra, J. J. Cowell and R. M. Lambert, *Catal. Lett.*, 2000, **67**, 87–91.
75 X. Y. Deng and C. M. Friend, *J. Am. Chem. Soc.*, 2005, **127**, 17178–17179.
76 C. Mukoid, S. Hawker, J. P. S. Badyal and R. M. Lambert, *Catal. Lett.*, 1990, **4**, 57–61.
77 J. T. Roberts, A. J. Capote and R. J. Madix, *J. Am. Chem. Soc.*, 1991, **113**, 9848–9851.
78 J. J. Cowell, A. K. Santra and R. M. Lambert, *J. Am. Chem. Soc.*, 2000, **122**, 2381–2382.
79 J. T. Roberts and R. J. Madix, *Surf. Sci.*, 1990, **226**, L71–L78.
80 S. Hawker, C. Mukoid, J. P. Baydal and R. M. Lambert, *Vacuum*, 1994, **45**, 275–278.
81 R. M. Lambert, F. J. Williams, R. L. Cropley and A. Palermo, *J. Mol. Catal. A: Chem.*, 2005, **228**, 27–33.
82 R. L. Cropley, F. J. Williams, A. J. Urquhart, O. P. H. Vaughan, M. S. Tikhov and R. M. Lambert, *J. Am. Chem. Soc.*, 2005, **127**, 6069–6076.
83 F. J. Williams, R. L. Cropley, O. P. H. Vaughan, A. J. Urquhart, M. S. Tikhov, C. Kolczewski, K. Hermann and R. M. Lambert, *J. Am. Chem. Soc.*, 2005, **127**, 17007–17011.
84 J. T. Gleaves, A. G. Sault, R. J. Madix and J. R. Ebner, *J. Catal.*, 1990, **121**, 202–218.
85 D. Pinnaduwage, L. Zhou, W. Gao and C. M. Friend, unpublished work.
86 M. A. Barteau, *Top. Catal.*, 2003, **22**, 3–8.
87 M. Enever, S. Linic, K. Uffalussy, J. M. Vohs and M. A. Barteau, *J. Phys. Chem. B*, 2005, **109**, 2227–2233.
88 D. Torres, N. Lopez, F. Illas and R. M. Lambert, *Angew. Chem., Int. Ed.*, 2007, **46**, 2055–2058.
89 S. Linic and M. A. Barteau, *J. Am. Chem. Soc.*, 2002, **124**, 310–317.
90 F. J. Williams, D. P. C. Bird, A. Palermo, A. K. Santra and R. M. Lambert, *J. Am. Chem. Soc.*, 2004, **126**, 8509–8514.
91 L. Zhou and R. J. Madix, unpublished work.
92 F. Jensen, F. Besenbacher and I. Stensgaard, *Surf. Sci.*, 1992, **270**, 400–404.
93 J. T. Roberts, A. J. Capote and R. J. Madix, *Surf. Sci.*, 1991, **253**, 13–23.
94 J. R. Monnier, J. W. Medlin and M. A. Barteau, *J. Catal.*, 2001, **203**, 362–368.

95 J. R. Monnier, J. L. Stavinoha and R. L. Minga, *J. Catal.*, 2004, **226**, 401–409.
96 J. R. Monnier, K. T. Peters and G. W. Hartley, *J. Catal.*, 2004, **225**, 374–380.
97 M. A. Barteau and R. J. Madix, *J. Am. Chem. Soc.*, 1983, **105**, 344–349.
98 J. T. Roberts, R. J. Madix and W. W. Crew, *J. Catal.*, 1993, **141**, 300–307.
99 C. R. Ayre and R. J. Madix, *Surf. Sci.*, 1992, **262**, 51–67.
100 W. X. Huang and J. M. White, *Catal. Lett.*, 2002, **84**, 143–146.
101 B. K. Min, X. Y. Deng, X. Y. Liu, A. R. Alemozafar, D. Pinnaduwage and C. M. Friend, unpublished work.
102 K. A. Davis and D. W. Goodman, *J. Phys. Chem. B*, 2000, **104**, 8557–8562.
103 X. Y. Liu and C. M. Friend, *J. Phys. Chem. C*, submitted.
104 X. Y. Liu, T. A. Baker and C. M. Friend, unpublished work.
105 T. S. Askgaard, J. K. Norskov, C. V. Ovesen and P. Stoltze, *J. Catal.*, 1995, **156**, 229–242.
106 C. V. Ovesen, B. S. Clausen, J. Schiotz, P. Stoltze, H. Topsoe and J. K. Norskov, *J. Catal.*, 1997, **168**, 133–142.
107 K. Reuter and M. Scheffler, *Phys. Rev. B: Condens. Matter Mater. Phys.*, 2006, **73**, 045433.
108 M. Rieger, J. Rogal and K. Reuter, *Phys. Rev. Lett.*, 2008, **100**, 016105.
109 H. Over and M. Muhler, *Prog. Surf. Sci.*, 2003, **72**, 3–17.
110 M. Neurock, *J. Catal.*, 2003, **216**, 73–88.
111 P. Minary and M. E. Tuckerman, *J. Am. Chem. Soc.*, 2005, **127**, 1110–1111.
112 R. Iftimie, P. Minary and M. E. Tuckerman, *Proc. Natl. Acad. Sci. U. S. A.*, 2005, **102**, 6654–6659.
113 S. Linic and M. A. Barteau, *J. Am. Chem. Soc.*, 2003, **125**, 4034–4035.
114 I. E. Wachs, *Surf. Sci.*, 2003, **544**, 1–4.
115 J. A. Schwarz and R. J. Madix, *Surf. Sci.*, 1974, **46**, 317–341.
116 G. E. Gdowski, J. A. Fair and R. J. Madix, *Surf. Sci.*, 1983, **127**, 541–554.
117 S. Linic and M. A. Barteau, *J. Catal.*, 2003, **214**, 200–212.
118 M. L. Bocquet and D. Loffreda, *J. Am. Chem. Soc.*, 2005, **127**, 17207–17215.
119 S. Linic, J. Jankowiak and M. A. Barteau, *J. Catal.*, 2004, **224**, 489–493.
120 M. Witko, K. Hermann, D. Ricken, W. Stenzel, H. Conrad and A. M. Bradshaw, *Chem. Phys.*, 1993, **177**, 363–371.
121 G. Papoian, J. K. Norskov and R. Hoffmann, *J. Am. Chem. Soc.*, 2000, **122**, 4129–4144.
122 B. Flemmig, I. Kretzschmar, C. M. Friend and R. Hoffmann, *J. Phys. Chem. A*, 2004, **108**, 2972–2981.
123 G. S. Jones, M. Mavrikakis, M. A. Barteau and J. M. Vohs, *J. Am. Chem. Soc.*, 1998, **120**, 3196–3204.
124 S. Linic, H. Piao, K. Adib and M. A. Barteau, *Angew. Chem., Int. Ed.*, 2004, **43**, 2918–2921.
125 M. L. Bocquet, A. Michaelides, D. Loffreda, P. Sautet, A. Alavi and D. A. King, *J. Am. Chem. Soc.*, 2003, **125**, 5620–5621.
126 D. Torres and F. Illas, *J. Phys. Chem. B*, 2006, **110**, 13310–13313.
127 D. Torres, N. Lopez and F. Illas, *J. Catal.*, 2006, **243**, 404–409.
128 A. Kokalj, P. Gava, S. de Gironcoli and S. Baroni, *J. Phys. Chem. C*, 2008, **112**, 1019–1027.
129 J. Greeley and M. Mavrikakis, *J. Phys. Chem. C*, 2007, **111**, 7992–7999.
130 D. Torres, N. Lopez, F. Illas and R. M. Lambert, *J. Am. Chem. Soc.*, 2005, **127**, 10774–10775.
131 L. Zhou, W. W. Gao, A. Klust and R. J. Madix, *J. Chem. Phys.*, 2008, **128**, 054703.
132 C. Kolczewski, F. J. Williams, R. L. Cropley, O. P. H. Vaughan, A. J. Urquhart, M. S. Tikhov, R. M. Lambert and K. Hermann, *J. Chem. Phys.*, 2006, **125**, 034701.